Non-Gaussian effects on hydraulic conductivity upscaling in unsaturated porous media via direct averaging

Rafael Leonardo Sandoval Pabon

Universidad Nacional de Colombia
School of Engineering
Graduate Programs in Civil and Agricultural Engineering
Bogotá DC, Colombia
2018

Non-Gaussian effects on hydraulic conductivity upscaling in unsaturated porous media via direct averaging

Rafael Leonardo Sandoval Pabón

Research Thesis presented as partial requirement to aim for the title:
Master of Science in Water Resources Engineering

Advisor:
Prof. Leonardo David Donado Garzón
Associate Professor

Research Line:
Applied Hydrogeology
Research Group:
Hydrodynamics of the natural media - HYDS

Universidad Nacional de Colombia
School of Engineering
Graduate Programs in Civil and Agricultural Engineering
Bogotá DC, Colombia
2018

A mi Madre, mujer que siempre me ha demostrado su incondicional amor

Aknowledgments

Special thanks to the support and guidance given by professors Monica Riva and Alberto Guadagnini from the Politecnico di Milano (Italy). Also, to members of Hydrodynamics of Natural Media - HYDS and GIREH research groups whose questions, discussions, and examples gave me new ideas to improve each part of this work. Finally, thanks to own international mobility programs of the National University of Colombia that partially found global mobilities.

Resumen

La conductividad hidráulica es un parametro clave en los procesos de flujo en el medio geológico. En este trabajo, la conductividad hidráulica no saturada fue escalada con el objetivo de determinar el valor óptimo del parámetro p (del método de escalado basado en promedios de potencias) que minimice la diferencia entre la carga hidráulica media calculada empleando un campo de conductividades fino y la carga hidráulica media calculada con un campo de conductividades escalado en un problema bidimensional de infiltración. Se empleó un enfoque probabilistico en el que la conductividad hidráulica se entiende como un proceso aleatorio en el espacio. Para escalar los campos de conductividad hidráulica se probaron valores del parámetro p que se encontraran dentro del intervalo [-1,1] y se trabajaron cuatro tasas de infiltración diferentes. Campos Gaussianos y no Gaussianos de conductividad hidráulica fueros analizados. Se encontró que el valor óptimo del parámetro p se encuentra entre la media geométrica y la media armonica para cualquier tasa de infiltración. Como resultado, valores óptimos del parametro p pueden disminuir el error en la carga hidráulica casi a la mitad, dependiendo de la tasa de infiltración del problema y el tipo de campos empleados.

Keywords: Hidrogeología, medio poroso, conductividad hidráulica, zona no saturada, ecuación de Richads, ley de Darcy, escalamiento, campos no Gaussianos, media generalizada

Abstract

Hydraulic conductivity is a key parameter governing groundwater flow processes. In this work, hydraulic conductivity was upscaled with the objective of assessing the optimal value of the p-power parameter (of the power averaging upscaling approach) that minimizes the discrepancy between the capillary pressure calculated with fine hydraulic conductivity fields, and the capillary pressure computed with upscaled fields in a two-dimensional unsaturated infiltration problem. The analyses were framed in a probabilistic context, where hydraulic conductivity is conceptualized as a random process in space. Values of p in the interval [-1,1] to scale the hydraulic conductivity under four different infiltration rates were tested. Gaussian and non-Gaussian random hydraulic conductivity fields were analyzed. An optimum p between geometric and harmonic means was found for all the infiltration rates. As a result, the optimum p-power can diminish the capillary pressure error almost to the half, depending on the infiltration rate of the problem and the employed fields.

Keywords: Hydrogeology, porous media, hydraulic conductivity, unsaturated zone, Richards equation, Darcy's law, upscaling, non-gaussian fields, generalized mean.

Contents

Aknowledgments **vii**

Resumen **ix**

Abstract **x**

1. Introduction **2**

2. Overview of Basic Concepts **6**

2.1. Groundwater 6

2.1.1. Porosity 6

2.1.2. Permeability and hydraulic conductivity 7

2.2. Unsaturated Zone Flow 8

2.2.1. Darcy's Law 8

2.2.2. Richards equation 8

2.2.3. Saturation functions 9

2.3. Numerical Simulation of Flow Problems 10

2.3.1. Spatial discretization schemes 10

2.3.2. Temporal discretization schemes 11

2.4. Random Fields Generation 11

2.4.1. Variogram 12

2.4.2. Gaussian fields 12

2.4.3. Sub-Gaussian fields 12

2.4.4. Random field generation approach 14

2.5. Hydraulic Conductivity Upscaling 14

3. Soil Parameters and Numerical Setup **16**

3.1. Soil parameters 16

3.2. Domain and boundary conditions 17

3.2.1. Physical domain 17

3.2.2. Boundary and Initial conditions 18

3.3. Generation of random fields 18

3.3.1. Gaussian fields 19

3.3.2. Non-Gaussian fields 21

3.4. Top boundary condition computation . . . 22
3.5. Solution of the capillary pressure . . . 24
3.6. Flow through finite volume faces computation . . . 25
3.7. Hydraulic conductivity averaging . . . 26

4. Numerical Implementation and Results - Gaussian Fields 28
4.1. Mesh independence test . . . 28
4.2. Numerical simulation of coarser hydraulic conductivity fields . . . 29
4.2.1. Grid refinement level influence . . . 29
4.2.2. P-power influence . . . 32
4.2.3. Infiltration rate influence . . . 34

5. Numerical Implementation and Results - non-Gaussian Fields 41
5.1. Mesh independence test . . . 41
5.2. Numerical simulation of coarser hydraulic conductivity fields . . . 43
5.2.1. Grid refinement level . . . 43
5.2.2. p-power influence . . . 44
5.2.3. Infiltration rate influence . . . 45
5.2.4. Comparison between Gaussian and non-Gaussian fields . . . 46

6. Summary, Conclusions and Recomendations 48

A. Appendix: Experimental and analytical covariance functions of the generated fields 51
A.1. Gaussian fields . . . 51
A.2. Non-Gaussian fields $\alpha = 1.8$ . . . 53
A.3. Non-Gaussian fields $\alpha = 1.5$ . . . 54

B. Appendix: Capillary pressure and flux MARE for non-Gaussian fields 56
B.1. Non-Gaussian fields α=1.9 . . . 56
B.2. Non-Gaussian fields α=1.7 . . . 58
B.3. Non-Gaussian fields α=1.5 . . . 60
B.4. Non-Gaussian fields α=1.3 . . . 62

References 64

List of Figures

1-1. Hydraulic conductivity difference PDF between cells for different lags 3
1-2. Basic scheme of the difference between support and block scales. 4

2-1. Porous media basic scheme. 7
2-2. Usual hydraulic conductivity Gaussian distribution. 13
2-3. Increments of variables probability density function at different lags. 15

3-1. Hydraulic Conductivity Gaussian Field. 17
3-2. Gaussian fields X-direction experimental and analytical covariance function. 20
3-3. Gaussian fields Y-direction experimental and analytical covariance function. 20
3-4. Gaussian fields $y = x$-direction experimental and analytical covariance function. 21
3-5. Flow diagram of the infiltration rate calculation. 23
3-6. Flow through finite volume face scheme. 24
3-7. Hydraulic conductivity scaling 25
3-8. Hydraulic conductivity and mathematical grid scaling 27

4-1. Capillary pressure MARE against HCFES for p=-1 and h=-20m. Gray lines represent each one of the realizations and red line represents the average error of the realizations. 30
4-2. Capillary pressure MARE statistics against HCFES for p=-1 and h=-20m. . 30
4-3. Capillary pressure MARE against HCFES for p=-0.5 and h=-1m. 31
4-4. Flux MARE against HCFES for p=-0.5 and h=-1m. 31
4-5. Flux MARE against HCFES for p=-1 and h=-10m. 32
4-6. Capillary Pressure MARE against p and h=-1m for some HCFES. 33
4-7. Flux MARE against p parameter for $h = -20m$ and some of the HCFES. . . 34
4-8. Capillary pressure MARE against p for different infiltration rates and the bigger refinement level. 35
4-9. Capillary pressure MARE against p for different infiltration rates and the smaller grid refinement level. 36
4-10. Flux MARE against p for different infiltration rates and the smaller grid refinement level. 36
4-11. Capillary pressure MARE against p for some HCFES and all infiltration rates. 37
4-12. Flux MARE against p for some HCFES and all infiltration rates. 39

5-1. Capillary pressure MARE for non-Gaussian fields (α=1.8). 42
5-2. Flux MARE for non-Gaussian fields (α=1.8). 43
5-3. Capillary pressure MARE for non-Gaussian fields (α=1.2). 44
5-4. Flux MARE for non-Gaussian fields (α=1.2). 45
5-5. Capillary pressure MARE against HCFES for p=0 and h=-1m. 46
5-6. log-capillary pressure MARE against HCFES for p=1 and $h = -1m$. 47

A-1. Experimental and analytical covariance function of the Gaussian fields in the X-direction 51
A-2. Experimental and analytical covariance function of the Gaussian fields in the Y-direction 52
A-3. Experimental and analytical covariance function of the Gaussian fields in the $y = x$ direction 52
A-4. Experimental and analytical covariance function of the sub-Gaussian fields ($\alpha = 1.8$) in the x-direction 53
A-5. Experimental and analytical covariance function of the sub-Gaussian fields ($\alpha = 1.8$) in the y-direction 53
A-6. Experimental and analytical covariance function of the sub-Gaussian fields ($\alpha = 1.8$) in the $y = x$ direction 54
A-7. Experimental and analytical covariance function of the sub-Gaussian fields ($\alpha = 1.5$) in the x-direction 54
A-8. Experimental and analytical covariance function of the sub-Gaussian fields ($\alpha = 1.5$) in the y-direction 55
A-9. Experimental and analytical covariance function of the sub-Gaussian fields ($\alpha = 1.5$) in the $y = x$ direction 55

B-1. Capillary pressure MARE for non-Gaussian fields α=1.9 56
B-2. flux MARE for non-Gaussian fields α=1.9 57
B-3. Capillary pressure MARE for non-Gaussian fields α=1.7 58
B-4. flux MARE for non-Gaussian fields α=1.7 59
B-5. Capillary pressure MARE for non-Gaussian fields α=1.5 60
B-6. flux MARE for non-Gaussian fields α=1.5 61
B-7. Capillary pressure MARE for non-Gaussian fields α=1.3 62
B-8. flux MARE for non-Gaussian fields α=1.3 63

List of Tables

3-1. Mean and standard deviation of the parameters for the van Genuchten - Mualem model of hydraulic conductivity 16
3-2. Input parameters for the Gaussian field generation 19
3-3. Imposed and obtained parameters of the Gaussian random fields. 19
3-4. GSLIB input parameters for the fields generation of non-Gaussian fields . . . 22
3-5. Imposed and obtained parameters of the non-Gaussian random fields (Y'_{SG}) . 22
3-6. Mean infiltration rates (m/day) for each mean capillary pressure and different types of field generation 23

4-1. Capillary pressure MARE between results obtained with mathematical grids of 120x120 and 60x60 elements for the first five realizations of Gaussian fields. 29
4-2. Ratio between MARE at p=-0.5 and MARE at p=1 for some HCFES and different infiltration rates. 37
4-3. Difference between MARE obtained with $p - power = -0.5$ and MARE obtained with $p - power = 1$ for different hydraulic conductivity grids and different infiltration rates. 38

5-1. Capillary pressure MARE (%) between 120x120 and 60x60 mathematical grids for the first five realizations of non-Gaussian fields 41

1. Introduction

Groundwater studies usually are focused on the saturated zones, however, unsaturated zones are also of importance (Tindall & Kunkel, 1999). Many human activities as crop production, infiltration fields, landfills, and civil infrastructure foundations are executed mainly in the unsaturated zones. Besides, the unsaturated zone is essential due to its relation with the saturated region of the natural media, for example, alluvial aquifers usually are recharged from the water coming from the unsaturated zone.

Unsaturated flow problems can be solved with numerical simulations of the Richards equation (Richards, 1931). This equation is the product of the combination between continuity equation and Darcy's law (Darcy, 1856) and it requires hydraulic conductivity information which is a parameter governing groundwater flow processes. This parameter is heterogeneous in space, and this heterogeneity has a strong influence in solutions of flow simulations.

Due to cost and time limitations, hydraulic conductivity is not sampled in all points of a domain before the implementation of numerical flow simulations. Traditionally, the parameter is tested in some locations, and then, with geostatistical tools, the entire area is filled with values of the property, a discretized domain with values of a property in all its cells is known as a realization of the property (Rubin, 2003; Samper & Carrera, 1990).

Usually, due to the lack of certainty in the creation of a hydraulic conductivity realization, many realizations are performed to create as many equally probable realizations as possible (usually limited by computational costs). Then, numerical simulations of flow are performed for each one of the equally probable realizations, and therefore, the solution of the problem is given as the probability of obtaining a specific value of pressure (or capillary pressure) in a given position (Rubin, 2003; Samper & Carrera, 1990).

Many geostatistical tools have been designed to generate the realizations of a property with a Gaussian probability distribution. However, as reported in Riva et al. (2015), many environmental (and ecological, biological, physical, social and financial) variables exhibit non-Gaussian behaviors. This is, whereas distributions of the variable are at times slightly asymmetric with relatively mild peaks and tails, those of the variable increments tend to be symmetric with peaks that grow sharper, and tails that become heavier, as the separation distance (lag) between pairs of the variable values decreases.

Permeability and hydraulic conductivity variables and its increments have shown to have non-Gaussian behaviors (Painter, 1986; Riva et al., 2013; Liu & Molz, 1997). To generate hydraulic conductivity realizations, Riva et al. (2015) have developed a model for the generation of non-Gaussian realizations. This model allows to create with geostatistical tools, non-Gaussian realizations, in which, heavy tails of the variable increment of the probability density functions (*pdf*) are correctly represented. This is important because those tails control the distribution of extreme values which are of central interest in hydrology and many other fields.

Figure **1-1** shows frequency of hydraulic conductivity difference between cells of a realization for different lags. As explained before, for smaller lags the *pdf* has peaks that grow sharper, and tails that become heavier, as the separation distance (lag) between pairs of the variable values decreases. This behavior can be seen in Guadagnini et al. (2018) for porosity in a borehole. In addition Figure **1-1** shows the best Gaussian and non-Gaussian *pdf*. As it can be seen, non-Gaussian *pdf* captures more accurately frequency distribution than Gaussian *pdf*.

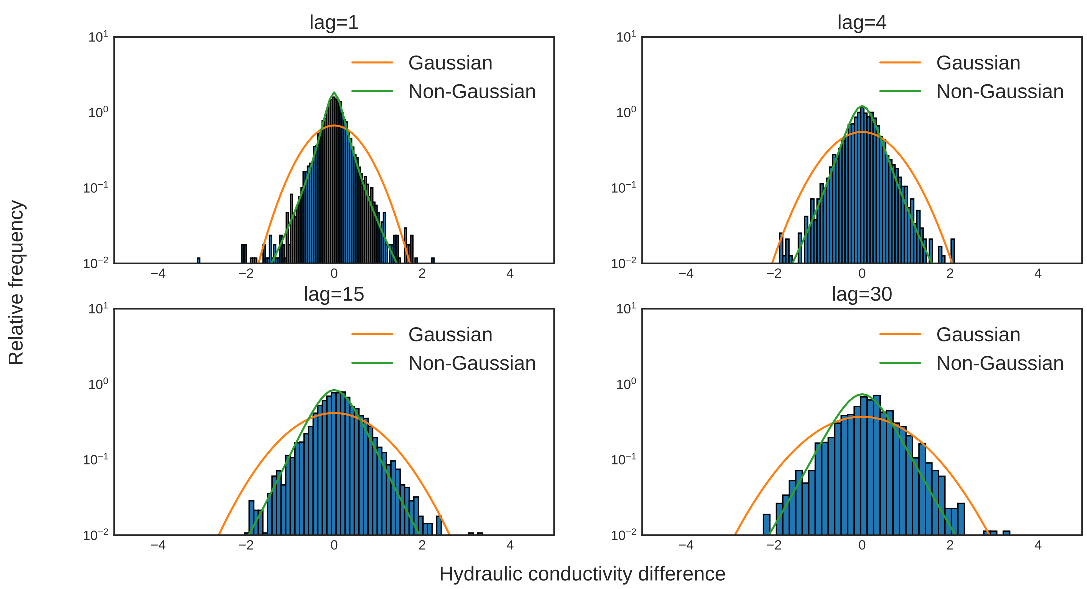

Figure 1-1.: Hydraulic conductivity difference PDF between cells for different lags

Once realizations of a property are performed, one could start the numerical flow simulations. However, due to computational costs, usually, the hydraulic conductivity support volume is smaller than the one used in flow models (Wen & Gomez-Hernandez, 1996). The latest makes imperative the scaling of hydraulic conductivity from measurement support scale to block scale (scale in which numerical simulations are performed) to perform accurate flow numerical simulations. Figure **1-2** shows a basic scheme of the support and block scales. Change of scale diminishes computational cost and thereby the time required for flow simulations.

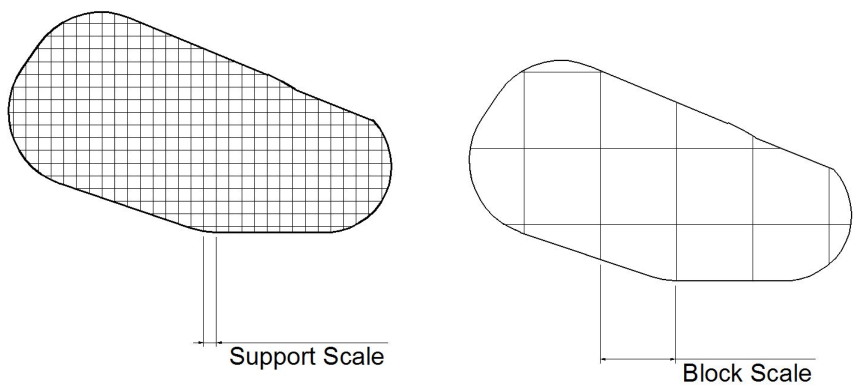

Figure 1-2.: Basic scheme of the difference between support and block scales.

A wide variety of methods could be used for scaling hydraulic conductivity. That includes local and non-local techniques, i.e., techniques that consider that block hydraulic conductivity are a function of cells within the block and methods that recognize the block hydraulic conductivity as a function of cells within and out of the block. Two of the most straightforward local scaling techniques are simple average and power average which consider the block conductivity as an average (harmonic, arithmetic, geometric and so on) of the cells within the block (Wen & Gomez-Hernandez, 1996).

Though scaling is a technique widely used in hydrogeology, its effects in numerical simulations of unsaturated flow simulations are not entirely known. Specifically, power average scaling has never been used in unsaturated flow numerical simulations looking for the optimum $p-power$ parameter. Besides, non-Gaussianity main effects in numerical simulations of unsaturated flow are not tested. This work pretends to advance in the comprehension of the non-Gaussianity and power average scaling in the unsaturated flow numerical simulations.

In this work, non-conditioned hydraulic conductivity realizations were generated with Gaussian and non-Gaussian probability density functions. Then, those hydraulic conductivity realizations were upscaled to perform non-saturated infiltration numerical simulations. Finally, the results of those simulations were compared with the real solution of the problem (taken as those produced with the finer hydraulic conductivity and mathematical grid). Influence of non-Gaussianity, $p - power$ parameter and infiltration rate in the solution of the simulations were evaluated.

It is important to note the limitations of this work, some of them are:

- Drying cycles are not taken into account during the simulations.
- Hysteresis is ignored.
- Stationarity in the mean is assumed.
- Ergodicity is assumed.
- It was not performed any experimental comparison.
- Comparisons were performed only for steady-state conditions.

The document is organized as follows: First, an overview of basic concepts is presented in section 2. Section 3 has the information related to the soil parameters and the numerical setup of the simulations. Results of the comparison between results obtained with different refinement levels, infiltration rates and p-power parameter with the real solution of the problems are shown in section 4. Section 5 has an overview of the comparison between the results of the simulations with different refinement levels, infiltration rates and p-power with the real solution of the problem. Section 7 discusses the most important results obtained in the work, conclusions, and recommendations. Finally, references and appendices are shown in the remaining sections.

2. Overview of Basic Concepts

This chapter presents some of the basic concepts related to the numerical simulation of flow in unsaturated media. It starts with a brief explanation of what is groundwater and some of its properties. Later a little review of equations governing unsaturated zone is shown. Then, concepts of spatial and temporal discretization schemes for flow simulations are presented. Next, it is shown an overview of the basic concepts to the generation of random fields. Finally, hydraulic conductivity upscaling is introduced.

2.1. Groundwater

Groundwater is the water that can be found into the geologic media in aquifers. An aquifer is a geologic formation or a group of formations which contains water and allows significant amounts of water to move through it. Such water is located in large areas; however, its utilization usually is concentrated to punctually located springs or facilities. Its seasonal variation is relatively small and can be easily monitored with groundwater level measurements (Bear, 2012). In porous media, water is inside the void spaces formed by the accommodation of discrete particles of geologic material (Figure **2-1**). In fractured media, water is located between the spaces formed by the fractures of impermeable (or almost impermeable) geologic media. Finally, in Karst, spaces and cavities are created into water-soluble materials by the continuous action of water over them.

Management of groundwater systems is the primary goal of a groundwater hydrologist. Because of that, numerical models are usually employed to obtain decision variables values useful to make decisions and apply policies in a region (Bear, 2012; Fetter, 1994; Domenico & Schwartz, 1997). Before numerical simulations, some soil and water aspects must be known, below the most important are shown:

2.1.1. Porosity

Porosity is the ratio between the void space in a geologic formation and the total volume. This parameter can range from values near to zero to values up to 60%. In general, for sedimentary materials, the smaller the particle size, the higher the porosity. Porosity can be expressed in two different ways: Total porosity and effective porosity. Total porosity

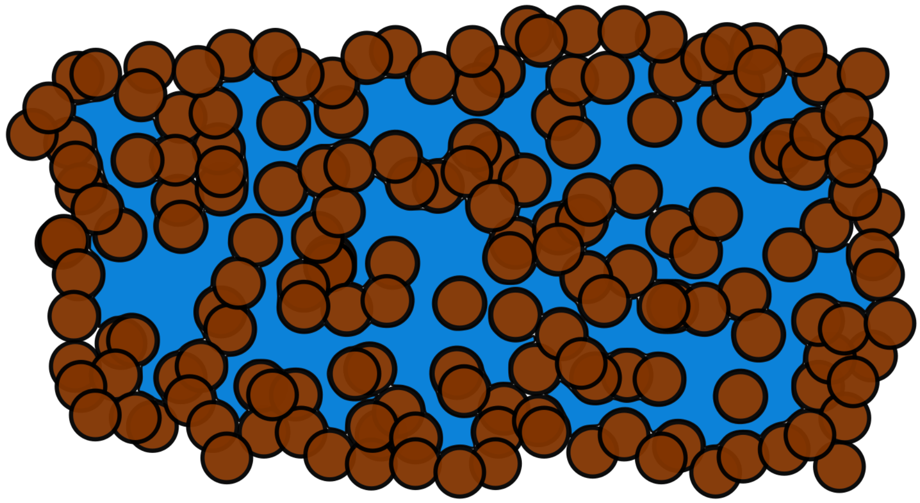

Figure 2-1.: Porous media basic scheme.

refers to the total void space in a geologic media whereas effective porosity is the volume of the interconnected void spaces (Domenico & Schwartz, 1997). For simplicity, this work will assume that values of total and effective porosity coincide.

2.1.2. Permeability and hydraulic conductivity

Permeability is the ease with which any fluid moves through geologic media. Intrinsic permeability is a function of the size of the pore opening. The smaller the size of the sediments grains, the larger the surface area and therefore, the higher the frictional resistance to flow which reduces the intrinsic permeability (Fetter, 1994).

Whereas permeability refers to the spaces through which any substance can flow, hydraulic permeability introduces the influence of the fluid. Then, permeability is a function of the soil, and hydraulic conductivity is a function of both: soil and fluid. Formally, hydraulic conductivity is the ease with which water can flow through geologic media, it is defined as in Equation 2-1, where K is the hydraulic conductivity $[L^2\ T^{-1}]$, k is the permeability $[L^2]$, ρ is the mass density of the fluid $[M\ L^3]$, g is the acceleration of the gravity $[L\ T^{-2}]$ and μ is the dynamic viscosity of the water $[M\ L^{-1}\ T^{-1}]$ (Fetter, 1994).

$$K = k\,\frac{\rho g}{\mu}. \tag{2-1}$$

2.2. Unsaturated Zone Flow

Flow in the geologic media has been studied from decades. Particularly, unsaturated zone most famous equation was proposed in 1931 by Lorenzo Richards (Richards, 1931). However, it is important to underline that there are other tools to solve flow problems in the unsaturated zone. Some of them are the Navier-Stokes equations; however, its application makes necessary a detailed spatial knowledge of the medium (usually not known in real field applications). Also, those equations demand a massive time of computation, making its application not viable for real field applications. Therefore, the Richards equation has been widely used for practical purposes. Bellow are explained some of the fundamentals of flow through unsaturated porous media.

2.2.1. Darcy's Law

In 1856 Henry Darcy, a French engineer made one of the first experiments about the movement of water in the porous medium. He found that the rate of water flowing through a bed of a "given nature" is proportional to the difference in the height of the water between the beginning and the end of the bed and the area and inversely proportional to the length of the flow path. Darcy used the hydraulic conductivity as proportionality constant (Darcy, 1856). The latest is known as the Darcy's Law; it is shown in Equation 3-9. Where, Q $[L^3\ T^{-1}]$ is the flow crossing a given area A $[L^2]$, K is the hydraulic conductivity $[L^2\ T^{-1}]$, h_A and h_B are the height of the fluid at the beginning and the end of the path respectively $[L]$ and L is the length of the flow path $[L]$ (Fetter, 1994).

$$Q = -K\ A\left(\frac{h_A - h_B}{L}\right). \tag{2-2}$$

Darcy's law can be written in more general terms as in equation 2-3, where $\partial H/\partial L$ is the hydraulic gradient.

$$Q = -K\ A\left(\frac{\partial H}{\partial L}\right). \tag{2-3}$$

2.2.2. Richards equation

A widely used model to represent flow in unsaturated porous media is the Richards equation (Richards, 1931). This model comes up as a combination of the continuity equation and Darcy's law. Bellow is the derivation of the Richards equation for the vertical direction.

Conservation of mass states that change in mass (in this specific case moisture) in a closed system is equal to the rate of change of the total sum of fluxes into and out of that volume:

$$\frac{\partial \theta}{\partial t} = \nabla \cdot \left(\sum_{i=1}^{n} q_{i,in} - \sum_{j=1}^{m} q_{j,out} \right). \tag{2-4}$$

Where θ is the soil moisture, t $[T]$ is time, $q_{i,in}$ $[LT^{-1}]$ is the inlet flow trough face i and $q_{i,out}$ $[LT^{-1}]$ is the outlet flow trough face j. In the vertical direction equation 2-4 can be written as:

$$\frac{\partial \theta}{\partial t} = -\frac{\partial q}{\partial z}. \tag{2-5}$$

Where z $[L]$ is the vertical dimension and q $[LT^{-1}]$ is the specific flow, this is, flow per unit of area. Specific flow can be expressed with Darcy's law, so:

$$\frac{\partial \theta}{\partial t} = -\frac{\partial}{\partial z} \left[-K \frac{\partial H}{\partial z} \right]. \tag{2-6}$$

Where K $[LT^{-1}]$ is the hydraulic conductivity and H $[L]$ is the hydraulic head. Substituting for $H = h + z$ (h $[L]$ being piezometric head):

$$\frac{\partial \theta}{\partial t} = \frac{\partial}{\partial z} \left[K \left(\frac{\partial h}{\partial z} + 1 \right) \right]. \tag{2-7}$$

The last is the mixed form of Richard's equation (Celia et al., 1990); this is because the water content is represented as two different physical quantities: volumetric saturation (θ) and hydraulic pressure (or capillary pressure) h. Richards equation is a non-linear hyperbolic partial differential with a hysteric parameter (Hydraulic conductivity). This means that the value of hydraulic conductivity varies for the same soil moisture depending if the soil is being dried or wetted. All those conditions make Richards equation a complicated model to simulate numerically. In this work was employed one of the most known saturation function, that ignores hydraulic conductivity hysteresis.

2.2.3. Saturation functions

Variation of hydraulic conductivity against water content and capillary pressure has a wide variety of constitutive models. Two of the most known models are the model of Brooks & Corey (1964) and the model of Van Genuchten (1980) based on the porous distribution model of Mualem (1976). Brooks and Corey model is shown in Equations 2-8, 2-9 and 2-10. Where, S_e is the effective saturation, α $[L^{-1}]$ is the inverse of the air-entry pressure, ψ $[L^{-1}]$ is the capillary pressure, n is a pore size distribution index, K $[LT^{-1}]$ is the hydraulic conductivity, K_s $[LT^{-1}]$ is the saturated hydraulic conductivity, θ is the volumetric water content, θ_s is the volumetric water content at saturation and θ_r is the residual volumetric water content.

$$S_e = \begin{cases} |\alpha\psi|^n & if \quad \psi < -1/\alpha \\ 1 & if \quad \psi \geq -1/\alpha \end{cases} \tag{2-8}$$

$$K = K_s S_e^{2/n+l+2} \tag{2-9}$$

$$S_e = \frac{\theta - \theta_r}{\theta_s - \theta_r} \tag{2-10}$$

Mualem - Van Genuchten model is shown in Equations 2-11 and 2-12, this is a model for rigid skeleton which consider invariable in time the structure of the soil, where l is the porous connectivity index and $m = 1 - 1/n$ is an impirical constant. Other parameters are the same than those of the Brooks and Corey model.

$$\theta(\psi) = \begin{cases} \theta_r + \frac{\theta_s - \theta_r}{[1+|\alpha\psi|^n]^m} & if \quad \psi < 0 \\ \theta_s & if \quad \psi \geq 0 \end{cases} \tag{2-11}$$

$$K(\psi) = K_s S_e^l \left[1 - \left(1 - S_e^{1/m}\right)^m\right]^2 \tag{2-12}$$

2.3. Numerical Simulation of Flow Problems

2.3.1. Spatial discretization schemes

Space should be discretized in order to solve a partial differential equation with independent spatial variables. Most common spatial discretization schemes are finite differences, finite elements, and finite volumes. In this work, finite volumes method will be used.

Finite Volumes Method

Finite volumes method for spatial discretization of a domain consists in the subdivision of the solution domain into small control volumes. Each control volume has a center in which information is concentrated and faces thought which data is transmitted in the form of flux (Ferziger & Peric, 2002). Equation 2-13 is the integral form of the mass conservation equation, where, t $[T]$ is time A is the quantity that varies (volumetric water content), V_n $[L^3]$ is the volume of the control volume, F_j $[L^{-2}T^{-1}]$ is the flux across the superficial area of the finite volume and $Q_j[T^{-1}]$ is a source/sink term.

$$\frac{\partial}{\partial t}\int_{V_n} A_j dV + \int_{V_n} \nabla \cdot F_j dV = \int_{V_n} Q_j dV \tag{2-13}$$

The second term could be changed to a surface integral using the Gauss theorem. Besides, it could be expressed as the sum of the flux through each face. So, mass conservation equation turns into Equation 2-14, here F_{jm} $[L^{-2}T^{-1}]$ is the flux through a finite volume in the face m and S_m $[L^2]$ is the superficial area of the finite volume in the face m. In porous media, the flux of moisture between two adjacent finite volumes could be calculated with Darcy's law. As Darcy's law requires a value of the hydraulic conductivity, usually it is computed as the interpolation of the two neighboring hydraulic conductivity values.

$$\frac{\partial}{\partial t}\int_{V_n} A_j dV + \sum_{i=1}^{m} F_{jm} S_m = \int_{V_n} Q_j dV \tag{2-14}$$

2.3.2. Temporal discretization schemes

As spatial discretization schemes, there exist multiple temporal discretization schemes like two-level methods, Predictor-corrector method or Runge-Kutta methods. However, in this work, it will be used a fully implicit Euler approach (two-level method).

Implicit Euler Approach

Implicit Euler method evaluates the variable values in the time $t + \Delta t$, this makes it an implicit method and therefore it is required to solve the entire domain values at the same time. This can be seen in Equation 2-15, where, fluxes and source/sink terms are calculated with the information in the time $t + \Delta t$.

$$\frac{A_n^{t+\Delta t} - A_n^t}{\Delta t} V_n + \sum_{i=1}^{m} F_{jm}^{t+\Delta t} S_m = \int_{V_n} Q_j^{t+\Delta t} dV. \tag{2-15}$$

2.4. Random Fields Generation

Numerical flow simulations require complete fields of hydraulic conductivity. However, due to the impossibility of sample an entire domain, geostatistical tools are employed to generate those fields. To represent the variability of the natural media accurately, it is common to create multiple realizations and therefore to compute numerous solutions for the same problem. It means that the problem is not anymore solved with a deterministic approach but with a probabilistic approach. In other words, the solution of the problem (capillary pressure and flux) is given as the probability of obtaining a specific value in a given position (Rubin, 2003; Samper & Carrera, 1990).

2.4.1. Variogram

To generate realizations of a parameter, it is necessary to characterize geostatistically its spatial behavior. One of the most used geostatistical tools is the variogram. A variogram is a function that quantifies the spatial correlation structure of a variable. In other words, a function that explains the variations of a parameter in space as a function of the separation distance (lag). Variogram should be computed with experimental data and then adjusted to a theoretical model. Most common variogram models are spheric, exponential and Gaussian variograms (Samper & Carrera, 1990). In this work the exponential variogram was employeed, a model that represents continuous phenomena, this is, variables in which variations between adjacent points are not huge.

A variogram gives important information about the spatial behavior of a parameter, such as the correlation length (the distance at which on average there is not any correlation between two points).

2.4.2. Gaussian fields

Traditionally, the generation of random fields is made with Gaussian fields. Fields whose probability density function is well represented with a Gaussian function (Equation 2-16 where Y is a random variable, σ^2 its variance and μ its mean). Figure **2-2** shows a usual log hydraulic conductivity distribution, specifically, one that corresponds to one of the Gaussian generated fields.

$$f(Y) = \frac{1}{\sqrt{2\pi\sigma^2}}\; e^{-\frac{(Y-\mu)^2}{2\sigma^2}} \tag{2-16}$$

2.4.3. Sub-Gaussian fields

Recently, a new model for the generation of non-Gaussian (or sub-Gaussian) fields was proposed by Riva et al. (2015). This model captures in a unified manner both, probability density functions of the variable and its increments with Equations 2-17 and 2-18 respectively, where Y is a zero-mean random function, α is a non-Gaussianity parameter that should be equal or lesser than 2 (being Gaussian for α=2), U is a non-negative random function independent of $G(x)$, $G(x)$ is a zero-mean Gaussian function and ΔY is the increment of Y.

$$f(Y) = \frac{1}{2\pi(2-\alpha)} \int_0^{\infty} \frac{1}{u^2}\; e^{-\frac{1}{2}\left(\frac{1}{(2-\alpha)^2} ln^2 \frac{u}{\sigma_G} + \frac{y^2}{u^2}\right)} du \tag{2-17}$$

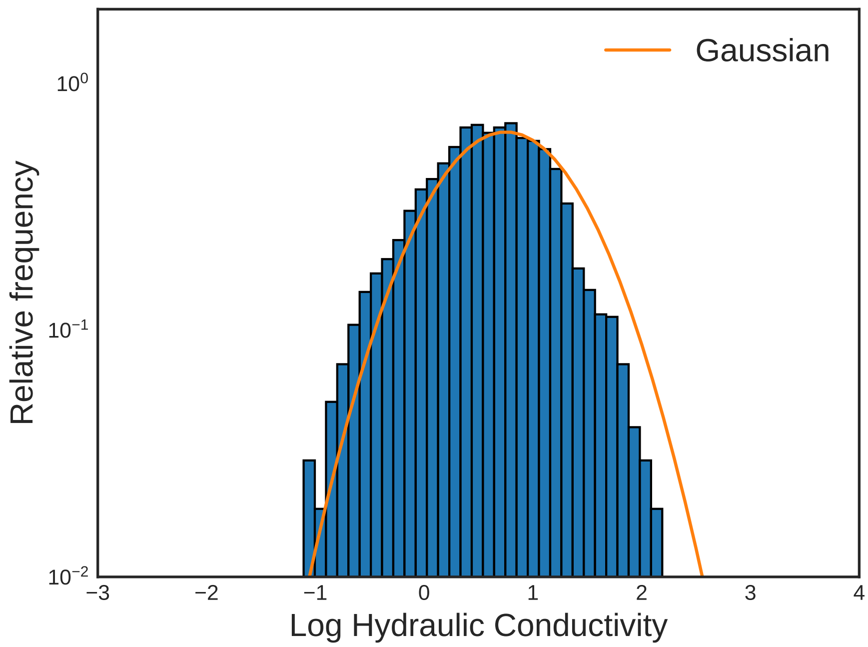

Figure 2-2.: Usual hydraulic conductivity Gaussian distribution.

$$f(\Delta Y) = \frac{1}{2\pi^2(2-\alpha)^2}\sqrt{\frac{\pi}{2}}\int_0^\infty \int_0^\infty \frac{e^{-\frac{1}{2}\left[\frac{1}{(2-\alpha^2)}\left(ln^2\frac{u_1}{\sigma_G}+ln^2\frac{u_2}{\sigma_G}\right)+\frac{(\Delta y)^2}{u_1^2+u_2^2-2u_1u_2\rho_G}\right]}}{u_2u_1\sqrt{u_1^2+u_2^2-2u_1u_2\rho_G}}du_2du_1 \tag{2-18}$$

The model allows generate fields with probability density functions similar to those found in environmental variables as a function of the α parameter, specially those of the variable increments. The latest can be seen in Figure **2-3** where, a frequency plot of the variable increments is plotted for four lags: 1, 4, 15 and 30 for one of the non-Gaussian realizations created with an α parameter equal to 1.5. Besides, Gaussian and non-Gaussian probability density functions are shown for each of the lags. As expected non-Gaussian functions fit much better to frequency plots than Gaussian fields. The latest is essential because real environmental variables probability density functions have the shape of the plots shown in Figure **2-3**. In other words, whereas distributions of the variable are at times slightly asymmetric with relatively mild peaks and tails, those of the variable increments tend to be symmetric with peaks that grow sharper, and tails that become heavier, as the separation distance (lag) between pairs of the variable values decreases.

2.4.4. Random field generation approach

Generation of random fields could be conditioned and unconditioned, this is, could be done with or without fixed values in the domain. In this work, GSLIB (Deutsch & Journel, 1998) was employed, it uses a sequential Gaussian simulation (SGSIM) to generate random fields. However, there exist multiple methods to make random fields, such as truncated Gaussian simulation, spectral method, turning bands method or simulated annealing simulation.

Sequential Gaussian Simulation Method

Sequential Gaussian simulation is an approach to perform (conditioned or unconditioned) random fields of a variable with a given mean, variance and variogram (Deutsch & Journel, 1998). Its algorithm is as follows:

1. Associate (if exists) hard data to the nearest cell.
2. Establish a random path through all the grid nodes.
3. Visit each grid node and find nearby data.
4. With the variogram construct by kriging the conditional distribution.
5. Draw simulated value.
6. Check the simulated value.

2.5. Hydraulic Conductivity Upscaling

Hydraulic conductivity upscaling is a method that transforms a grid of hydraulic conductivity defined at the scale of the measurements, into a coarser grid of block conductivities usable for input to a numerical flow simulator. Upscaling hydraulic conductivity is precise since usually there exist a disparity between the measurement scales and the scales at which aquifers are discretized for the numerical simulation of flow and transport. There exist a wide variety of upscaling methods; however, those can be classified into two principal groups: Local and nonlocal methods. i.e., techniques that consider that block hydraulic conductivity is a function of cells within the block and techniques that recognize the block hydraulic conductivity as a function of cells within and out of the block. Two of the most straightforward local scaling techniques are simple average and power average whose consider the block conductivity as an average (harmonic, arithmetic, geometric and so on) of the cells within the block (Wen & Gomez-Hernandez, 1996; Godoy et al., 2018). In this work, the averaging

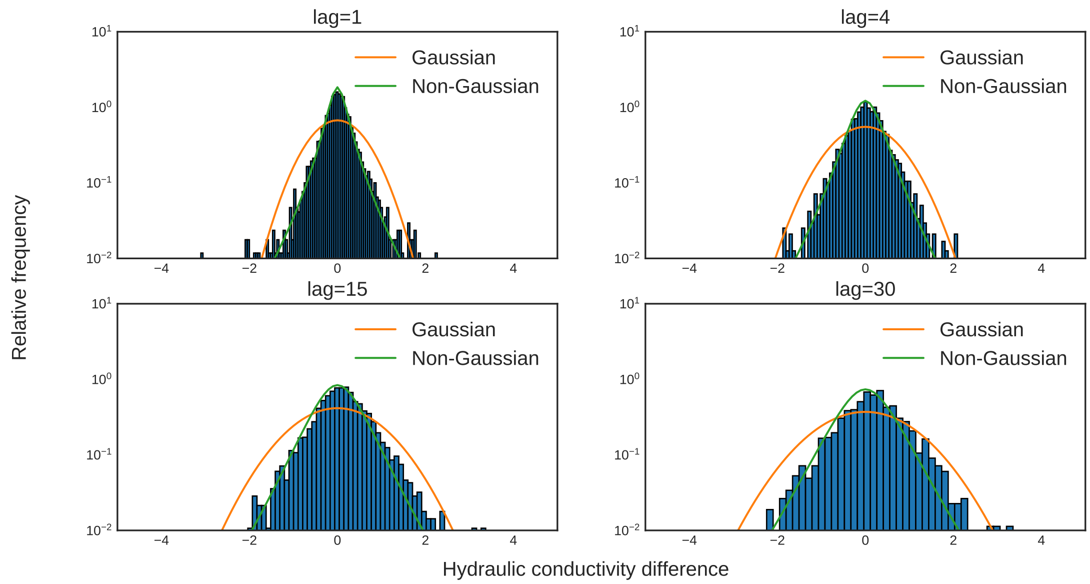

Figure 2-3.: Increments of variables probability density function at different lags.

method will be employed. It is properly explained in Section **3.7**.

This chapter has shown briefly some of the basic concepts related to the numerical simulation of flow in unsaturated media. It includes: Equations representing flow in unsaturated porous media and its treatment to perform numerical simulations; Geostatistic concepts to generate random fields and hydraulic conductivity upscaling.

3. Soil Parameters and Numerical Setup

This section of the work presents: Parameters of the soil employed for the field generations; Descriptions of the domain and the boundary conditions; Method of generation and verification of the random fields; Capillary pressure solution method; Flow computation method and upscaling method employed.

3.1. Soil parameters

The soil parameters used for the field generation correspond to those of the soil characterized and used by Khaleel (1999), mentioned parameters are based on laboratory measurements of moisture retention and unsaturated K for coarse-textured sandy samples from the upper Hanford formation at the Hanford Site, Washington. The mean and standard deviation of the van Genuchten - Mualem parameters of the soil used for the field generation can be seen in Table **3-1**. Same parameters were used by Khaleel et al. (2002).

Table 3-1.: Mean and standard deviation of the parameters for the van Genuchten - Mualem model of hydraulic conductivity

Parameter	**Mean**	**Standard Deviation**
$ln(K_s), m/day$	0.752	0.627
$ln(\alpha), 1/m$	1.460	0.341
$ln(n)$	0.600	0.089
θ_s	0.397	0.031
θ_r	0.027	0.004

Due to the purpose of this work (which is the scaling of the hydraulic conductivity) α, n, θ_s and θ_r are treated as deterministic constants. Hydraulic conductivity covariance is characterized by a two-dimensional exponential variogram (Equation 3-1) where γ is the covariance, σ^2 is the variance, λ_x and λ_y are the integral scales in x and y respectively and x and y are the horizontal and vertical directions. The correlation length (λ) of the exponential model is 5 m and 1 m for horizontal and vertical directions, respectively.

$$\gamma^2 = \sigma^2 \ e^{-\sqrt{\frac{x^2}{\lambda_x^2}+\frac{y^2}{\lambda_y^2}}}. \tag{3-1}$$

3.2. Domain and boundary conditions

3.2.1. Physical domain

The physical domain represented in this work is vertical, two-dimensional, 20 m wide and 20 m deep and it is discretized into 60 x 60 equally sized blocks. The medium within each block is considered as uniform. The figure **3-1** shows one of the Gaussian k (hydraulic conductivity) generated fields.

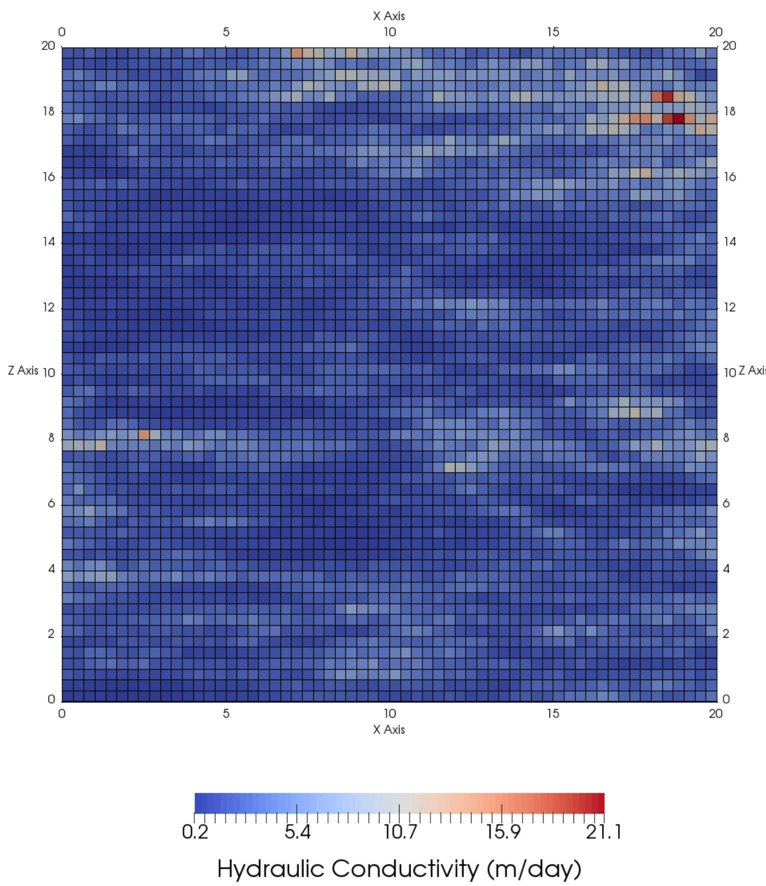

Figure 3-1.: Hydraulic Conductivity Gaussian Field.

3.2.2. Boundary and Initial conditions

No flow boundary conditions are imposed on the right and left sides of the domain (Equation 3-2, where h_i is the hydraulic head in i, P_i is the capillary pressure in i and x_i is the x coordinate in i). A free flow boundary condition is imposed to the bottom line of the field (Equation 3-3, where z_i is the z coordinate in i), this type of boundary condition implies that in the bottom boundary the flow is not affected by the capillary pressures of the elements but only by the height differences between volumes.

$$\frac{\partial h}{\partial x} \approx \frac{h_{i+1,j} - h_{i,j}}{x_{i+1,j} - x_{i,j}} = \frac{P_{i+1,j} - P_{i,j}}{x_{i+1,j} - x_{i,j}} = 0 \Rightarrow P_{i+1,j} = P_{i,j} \tag{3-2}$$

$$\frac{\partial h}{\partial z} \approx \frac{h_{i,j+1} - h_{i,j}}{z_{i,j+1} - z_{i,j}} = \frac{P_{i,j+1} + z_{i,j+1} - P_{i,j} - z_{i,j}}{z_{i,j+1} - z_{i,j}} = \frac{P_{i,j+1} - P_{i,j} + \Delta z}{\Delta z} = 1 \Rightarrow P_{i,j+1} = P_{i,j} \tag{3-3}$$

Finally, for the top boundary condition, an infiltration rate that produces a given mean capillary pressure when the problem has achieved steady-state conditions is computed and imposed. In other words, for a prescribed value of capillary pressure h_0, different infiltration rates are tested and the mean capillary pressure $\langle h \rangle$ (computed with Equation 3-4 in which n is the number of elements of the domain, and h_i is the capillary pressure in the cell i) is compared with the prescribed value of capillary pressure. Once the specified value of capillary pressure and the mean pressure head are close enough (maximum difference of 1%) the infiltration rate is taken as the upper boundary condition. As the calculated infiltration rate is a function of the field properties (especially hydraulic conductivity) and not of the ensemble, it is necessary to compute one infiltration rate for each realization. It means 50 different infiltration rates for each mean pressure head evaluated.

$$\langle h \rangle = \frac{1}{n} \sum_{i=1}^{i=n} h_i. \tag{3-4}$$

3.3. Generation of random fields

Generation of Gaussian and non-Gaussian hydraulic conductivity random fields was performed using the GSLIB (Geostatistical Software Library) package, developed by Deutsch & Journel (1998), with a Graphic User Interface (GUI). GSLIB consists in a group of free geostatistical tools written in Fortran and available to be used in most common operative systems. However, the GUI used in this work only runs in Windows.
GSLIB can perform simulations of random fields correlated in space under different covariance functions (Spherical, Exponential, Gaussian, Matèrn, Power Variogram and Truncated Power Variogram) and different spatial behaviors (anisotropy in correlation lengths,

anisotropy in angles, nugget effect, and conditional points). To generate Gaussian and non-Gaussian simulations, GSLIB employs the sequential Gaussian simulation method for the generation of random fields.

3.3.1. Gaussian fields

The parameters introduced in the GSLIB-GUI package for the Gaussian fields generation were: the covariance function, variance, dimensions of the fields, number of nodes, correlation lengths, nugget effect, and anisotropy angles. The parameters and its values are shown in Table **3-2**.

Table 3-2.: Input parameters for the Gaussian field generation

Parameter	Value
Covariance function	Exponential
Variance	0.393
Wide	20 m
Height	20 m
Nodes in x	60
Nodes in x	60
Correlation length x	5 m
Correlation length z	1 m
Nugget effect	0
Anisotropy angles	0

Before generated fields can be used, it is essential to check that they were correctly created. This is, to verify that the simulated mean, standard deviation and correlation lengths coincide with those imposed. For this reason, a set of 500 fields was created to check the correct generation of the imposed parameters. Table **3-3** shows the simulated and the imposed mean and variance average across the domain, the error is small and thereby, the mean and standard deviation are well reproduced.

Table 3-3.: Imposed and obtained parameters of the Gaussian random fields.

Parameter	Imposed	Obtained
Variance	0.393	0.383
Mean	0.000	0.002

Figure **3-2** represents covariance function in the x-direction, this plot has the experimental (dots) and theoretical (continuous line) covariance functions which are almost juxtaposed one over the other, this means that the correlation length in x is well represented. The same procedure was followed for the y (Figure **3-3**) and $y = x$ (Figure **3-4**) directions and similar behaviors were found, this means that the correlation length in the y-direction is well represented and therefore, the anisotropy as well.

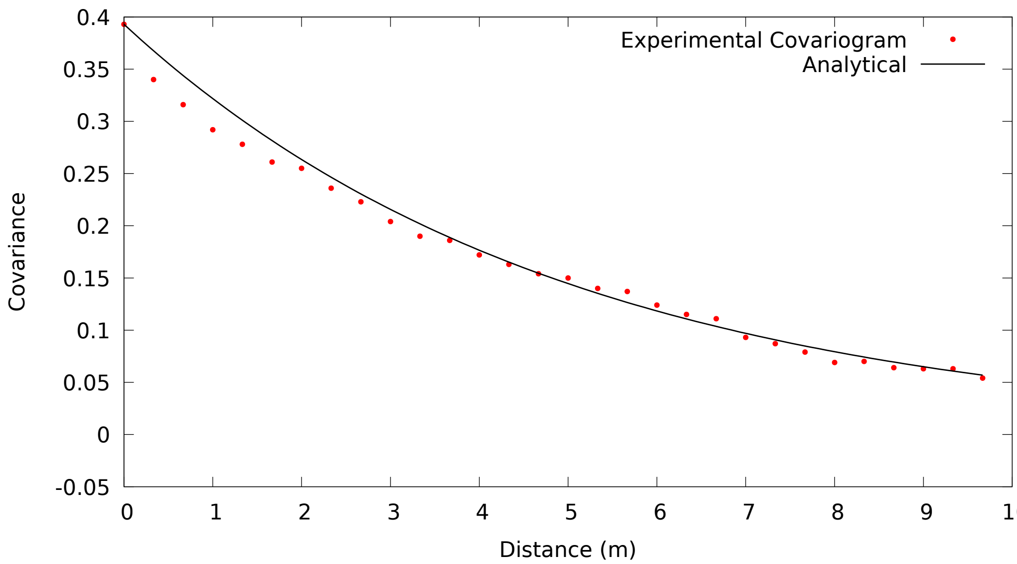

Figure 3-2.: Gaussian fields X-direction experimental and analytical covariance function.

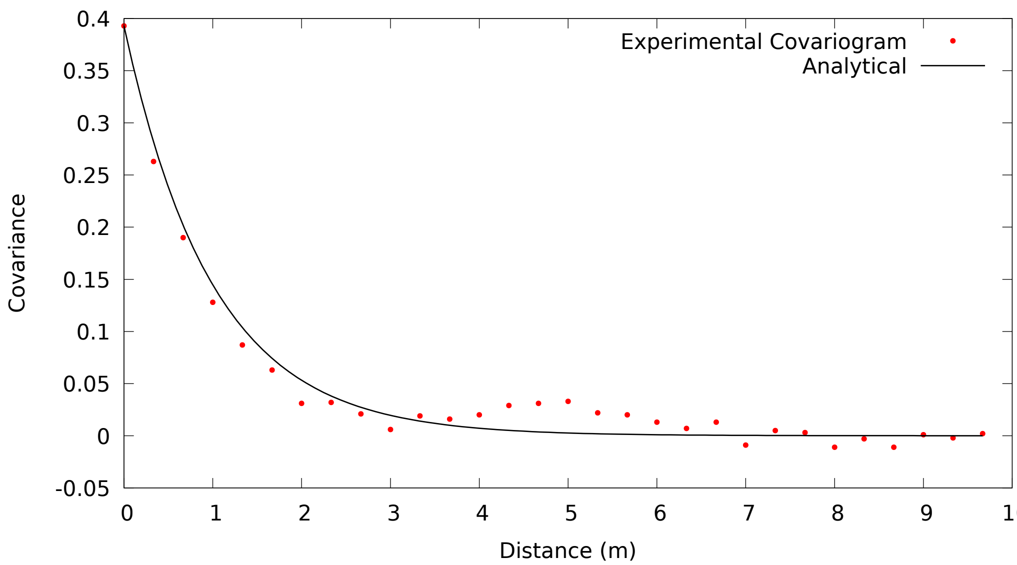

Figure 3-3.: Gaussian fields Y-direction experimental and analytical covariance function.

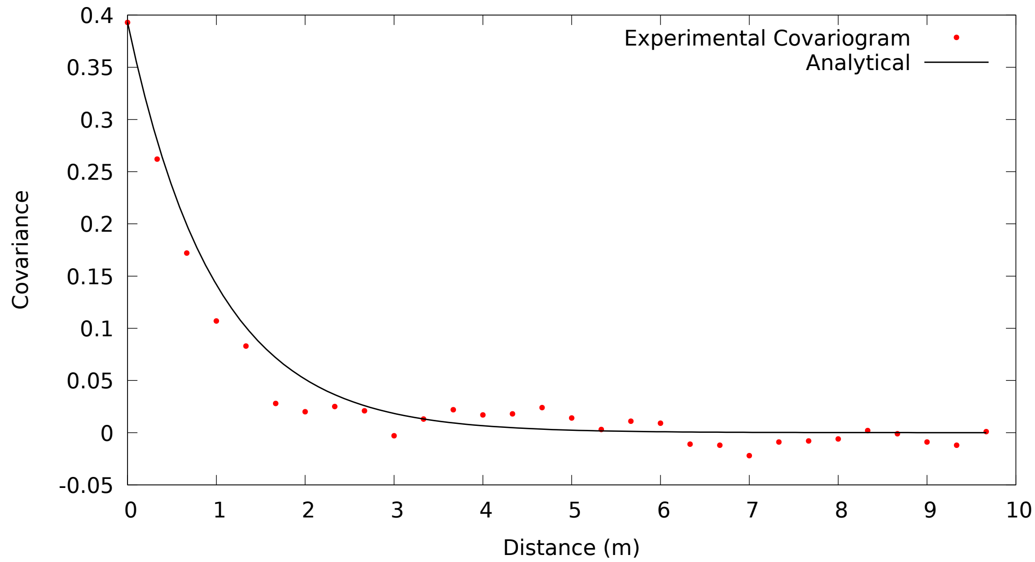

Figure 3-4.: Gaussian fields $y = x$-direction experimental and analytical covariance function.

3.3.2. Non-Gaussian fields

In order to generate with GSLIB the non-Gaussian fields of the model proposed by Riva et al. (2015), $Y(x) = G(x)U(x)$, input parameters of the zero-mean Gaussian distribution $G(x)$ and the α non-Gaussianity parameter are required. In this work, the random function $U(x)$ was selected as exponential, for this reason, the input parameters have to be calculated with the equations (3-5), (3-6) and (3-7) adopted from Riva et al. (2015) and Riva et al. (2017), where σ_G^2 is the variance of G, σ_Y^2 is the variance of Y, I_{G_x} and I_{G_z} are the integral scales of G in x and z directions respectively, I_{Y_x} and I_{Y_z} are the integral scales of Y in x and z directions respectively and α is the non-Gaussianity parameter. Here it is important to underline that Y (being non-Gaussian) must have the same mean, standard deviation and integral scales that the Gaussian fields.

$$\sigma_G^2 = \frac{\sigma_Y^2}{e^{2(2-\alpha)^2}} \tag{3-5}$$

$$I_{G_x} = \frac{I_{Y_x}}{e^{-(2-\alpha)^2}} \tag{3-6}$$

$$I_{G_z} = \frac{I_{Y_z}}{e^{-(2-\alpha)^2}} \tag{3-7}$$

The computed parameters for the zero-mean Gaussian distribution required to generate the non-Gaussian fields can be seen in table **3-4** for four different α values: 1.9, 1.8, 1.7 and 1.5.

Table 3-4.: GSLIB input parameters for the fields generation of non-Gaussian fields

Parameter	$\alpha = 1.8$	$\alpha = 1.5$	$\alpha = 1.2$
Variance	0.363	0.238	0.109
I_x	5.204	6.420	9.482
I_y	1.041	1.284	1.896

Like the Gaussian fields, non-Gaussian fields must be checked before being used. The same procedure used for the Gaussian fields was used to test the non-Gaussian fields. Table **3-5** shows the imposed and obtained mean and variance of the non-Gaussian fields. As for the Gaussian fields, the mean and variance are well represented by the generated fields. The correlation lengths and anisotropy were also checked and are correctly described as well; this can be seen in Appendix A.

Table 3-5.: Imposed and obtained parameters of the non-Gaussian random fields (Y'_{SG})

Parameter	**Imposed**	**Obtained**			
		1.9	**1.8**	**1.7**	**1.5**
Variance	0.393	0.381	0.384	0.384	0.381
Mean	0	-0.003	0.003	0.001	0.003

3.4. Top boundary condition computation

After the generation (and verification) of the Gaussian and non-Gaussian fields, the top boundary condition was calculated. For this, infiltration rates that produce four given mean capillary pressures (when the simulation reach steady-state conditions) were calculated for each field. i.e., when the simulations reach steady-state conditions, the capillary pressure of the domain cells are averaged and the mean capillary pressure must be close to a given capillary pressure (acceptable error of 1%). If the infiltration rate produces the desired mean capillary pressure, then the infiltration rate is adopted as the upper boundary condition, if not, the imposed infiltration rate is modified conveniently and the procedure starts again. A flow chart of the process is shown in Figure **3-5**.

As the infiltration rate computation is a function of the properties of each field and not of the ensemble properties, the infiltration rate should be computed for each field. Four different mean capillary pressures were selected: -20m, -10m, -5m and -1m. As a result, 50 infiltration rates were computed for each mean capillary pressure and each type of field (Gaussian and non-Gaussians). Table **3-6** shows for the four mean capillary pressure and the Gaussian and non-Gaussian fields the mean infiltration rate of the fields. From now on, mean capillary pressure and infiltration rate metrics will be used indistinctly.

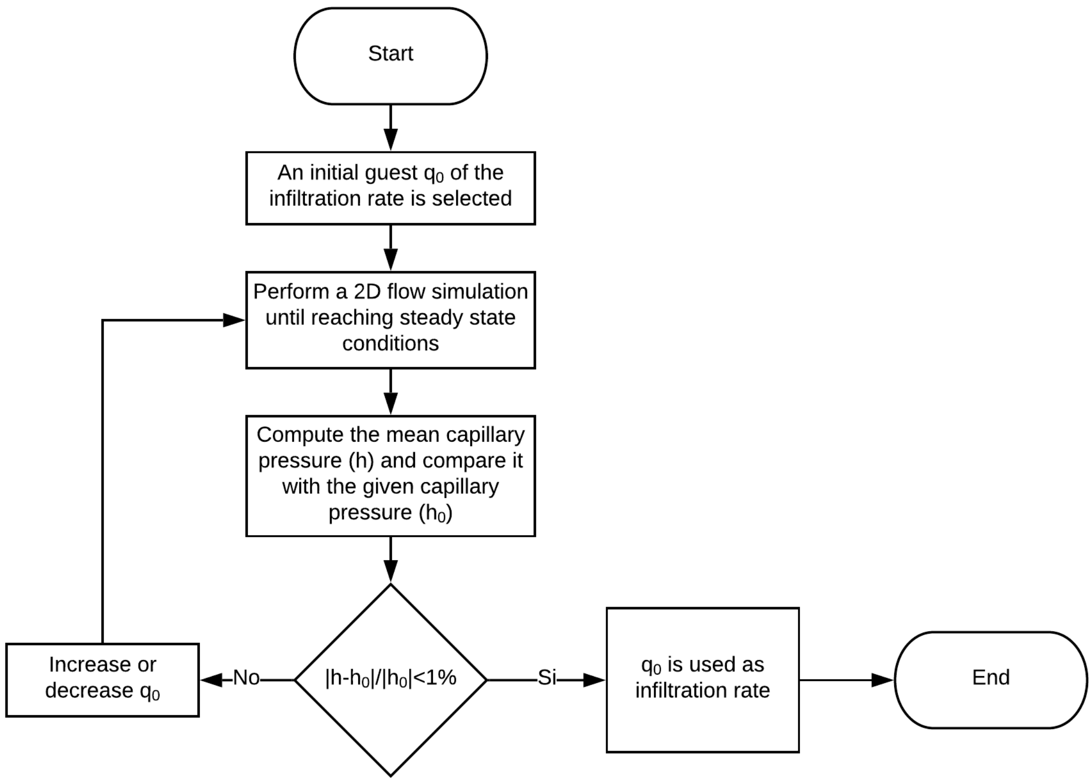

Figure 3-5.: Flow diagram of the infiltration rate calculation.

Table 3-6.: Mean infiltration rates (m/day) for each mean capillary pressure and different types of field generation

Mean capillary pressure (m)	**Gaussian Fields**	**Non-Gaussian** $\alpha = 1.9$	**Non-Gaussian** $\alpha = 1.8$	**Non-Gaussian** $\alpha = 1.7$	**Non-Gaussian** $\alpha = 1.5$
$h = -1$	1.131E-3	1.125E-3	1.163E-3	1.174E-3	1.120E-3
$h = -5$	1.756E-6	1.776E-6	1.841E-6	1.873E-6	1.793E-6
$h = -10$	1.039E-7	1.063E-7	1.102E-7	1.130E-7	1.077E-7
$h = -20$	6.338E-9	6.450E-9	6.737E-9	6.948E-9	6.596E-9

3.5. Solution of the capillary pressure

Once fields are generated and upper boundary conditions are computed, numerical simulations to calculate capillary pressure can be performed. For this, PFLOTRAN (Lichtner et al., 2017a,b), a massively parallel reactive flow and transport model for describing surface and subsurface processes was used. Specifically, for the solution of the posed problem, Richards mode of PFLOTRAN was employed, this mode applies to single phase, variably saturated and isothermal systems. Equations 3-8 and 3-9 are the governing mass conservation equation and Darcy flux respectively. 3-10 is the relative permeability equation.

$$\frac{\partial}{\partial t}(\phi s \eta) + \nabla \cdot (\eta q) = Q_w \tag{3-8}$$

$$q = -\frac{k\ k_r(s)}{\mu}(\nabla P - \rho g)\Delta x = -\frac{k\ k_{r_{up}}(s)}{\mu}\frac{[P_{dn} - P_{up} + \rho(g \cdot u)\Delta z]}{\Delta z}\Delta x \tag{3-9}$$

$$k_r = \sqrt{s_e}\left\{1 - [1 - (s_e)^{1/m}]^m\right\}^2 \tag{3-10}$$

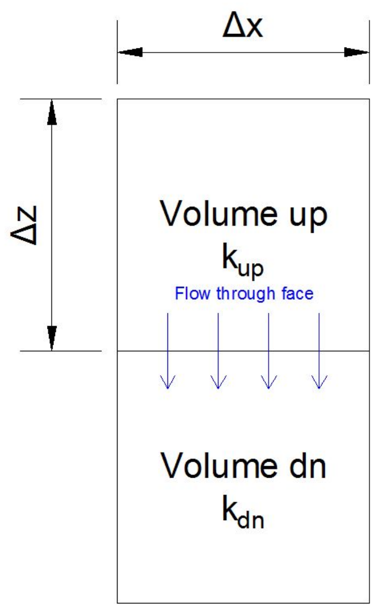

Figure 3-6.: Flow through finite volume face scheme.

Here, ϕ denotes volumetric porosity taken as 0.397; s saturation; η molar water density; $\mathbf{q}$ Darcy flux; Q_w a source/sink term, taken from the upper and bottom boundary conditions; k the intrinsic permeability, it was computed as the harmonic mean of the adjacent volumes; $k_{r_{up}}$ the upwinded relative permeability, calculated with the Mualem function based on the van Genuchten saturation function; μ is the dynamic viscosity, taken as $0.00089 Pa\ s$; P is the liquid pressure; ρ mass water density, taken as 996.78 kg/m^3; g is the gravity acceleration vector, taken as $9.81m/s^2$; Δz and Δx are the volume height and width respectively, both considered as 0.333 m, u is a vertical positive unitary vector, s_e is the effective saturation and m is an impirical constant .

PFLOTRAN employees finite volumes method as spatial discretization scheme and a fully implicit backward Euler approximation for the temporal discretization scheme, it means that the solution is unconditionally stable. Another reason why PFLOTRAN was used is due to its capability of accepting heterogeneous fields. In this work, HDF5 format files were used along PFLOTRAN to represent the heterogeneous hydraulic conductivity fields.

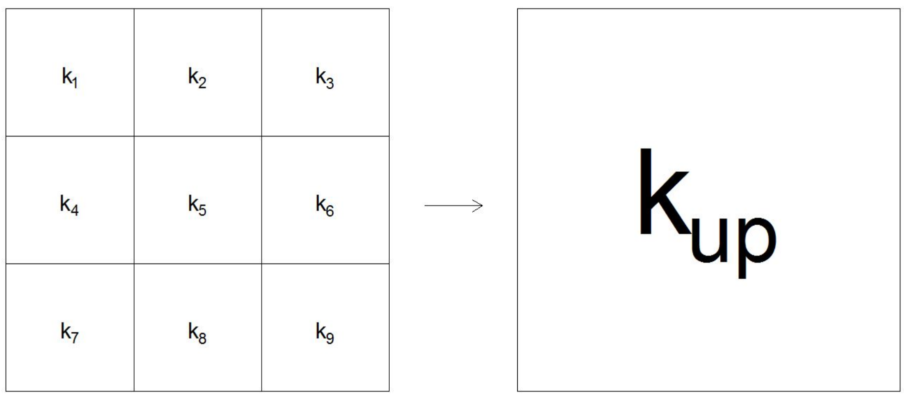

Figure 3-7.: Hydraulic conductivity scaling

3.6. Flow through finite volume faces computation

In addition to the capillary pressure, flux through finite volume faces is of interest. For this reason, once capillary pressure was computed in a field, flow through finite volume faces was computed for Gaussian and non-Gaussian fields. However, due to the boundary conditions of the problem, only vertical flows were computed, for this, Darcy velocity was calculated using the equation (3-9).

Figure **3-6** is a scheme of the properties used for the computation of the flow through a face and their respective origin. In there, it can be seen two adjacent finite volumes joined by a face. Though flow is not exclusively vertical, boundary conditions of the problem allow assuming that vertical flow is much higher than horizontal flow. Therefore, flow through lateral faces of each finite volume are not calculated. As relative permeability k_r is upwinded, it means that relative permeability used in the equation 3-9 is the one calculated in the volume-up. i.e., upstream relative permeability.

3.7. Hydraulic conductivity averaging

Equation 3-11 (where k_{up} is the upscaled hydraulic conductivity, n is the number of elements, k_i is the hydraulic conductivity at the fine scale and p is the scaling parameter) was used with 6 different p-powers (-1, -0.5, 0, 0.25, 0.5 and 1) in order to upscale the hydraulic conductivity Gaussian and non-Gaussian fields of 60x60 elements to obtain hydraulic conductivity grids of 30x30, 20x20, 15x15, 12x12, 10x10, 6x6, 5x5, 4x4, 3x3 and 2x2 elements. Figure **3-7** shows the typical procedure employed to scale hydraulic conductivity fields, in there, a zone of nine elements turns into a zone of just one element.

$$k_{up} = \left(\frac{1}{n} \sum_{i=1}^{n} k_i^p \right)^{1/p} \tag{3-11}$$

Even for the coarser hydraulic conductivity grid (2x2 elements), the mathematical grid was always of 60x60 elements in order to avoid two different sources of error (mathematical grid scaling and hydraulic conductivity scaling). Therefore, the computer error could be attributed solely to the scaling of the hydraulic conductivity fields. An example of this can be seen in Figure **3-8**, in there, it is shown the upscaling, in which, hydraulic conductivity field changes from a 60x60 elements grid to a 5x5 elements grid but the mathematical grid maintains the same refinement level (60x60 elements).

This section of the work has shown: Parameters of the soil employed for the field generations; Domain and boundary conditions descriptions; Method of generation and verification of the random fields; Solution method of the capillary pressure; Computation method to obtain flow and employed upscaling method. Next chapter will show the main results obtained from the scaling of hydraulic conductivity for Gaussian Fields.

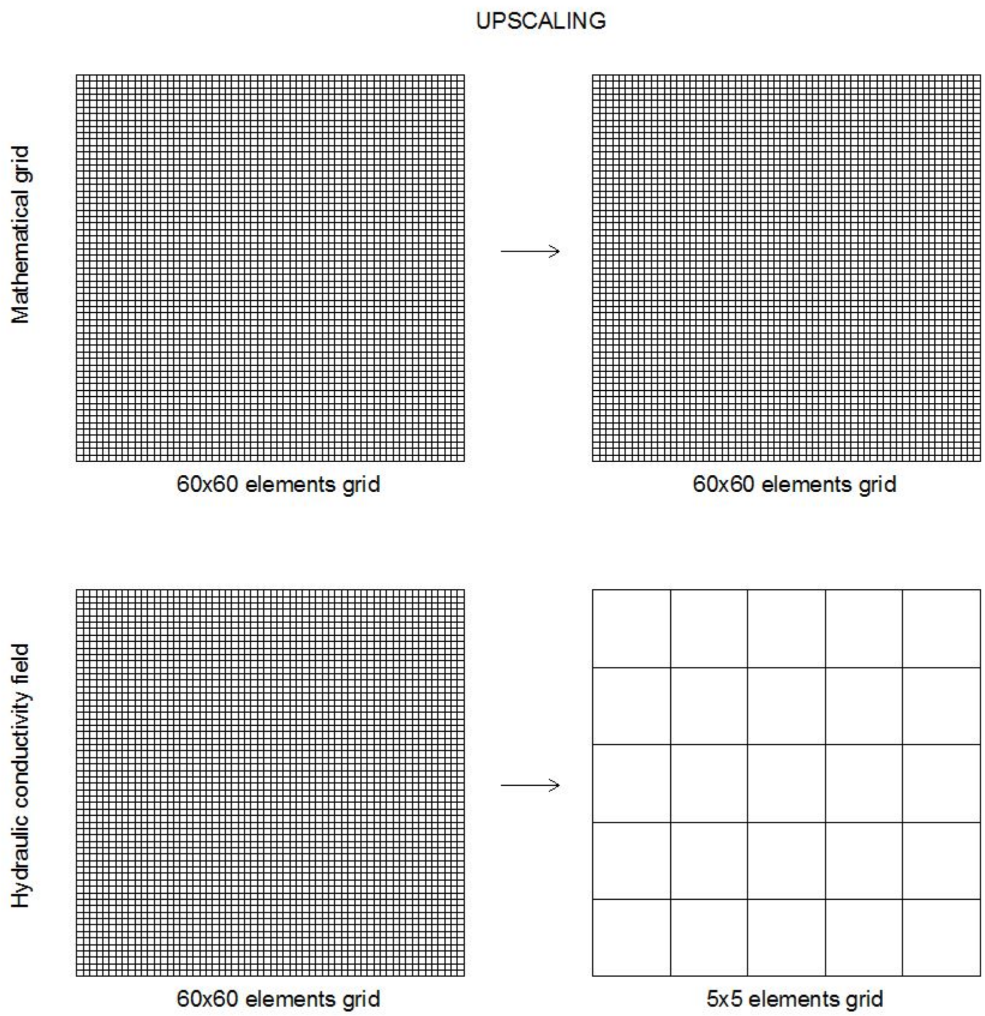

Figure 3-8.: Hydraulic conductivity and mathematical grid scaling

4. Numerical Implementation and Results - Gaussian Fields

With the Gaussian hydraulic conductivity fields already created and the boundary conditions of the problem established, numerical simulations of flow with original and upscaled fields can be performed. This chapter will show: a mesh independence test of the problem and a comparison between the results obtained with the upscaled fields and the real solution of the problem.

4.1. Mesh independence test

The capability of the generated fields to represent the phenomena simulated accurately with a numerical grid of 60x60 elements was evaluated. i.e., to assume that mathematical grids of 60x60 elements produce "real results", it is necessary to perform a mesh independence test. For Gaussian fields, simulations with the same boundary and initial conditions, same hydraulic conductivity grids, but with finer mathematical grids (120x120 elements) were performed and compared with those of 60x60 elements through a mean absolute relative error calculation (from now on called MARE) across the domain (equation 4-1). In the MARE equation, N is the number of finite volumes in the 60x60 area, h_{60_i} is the capillary pressure of the volume i in the 60x60 field and h_{120_i} is the arithmetic averaged capillary pressure of the 120x120 mathematical grid finite volumes juxtaposed over the 60x60 mathematical grid finite volume i.

$$MARE = \frac{1}{N}\sum_{i=1}^{i=N}\left|\frac{h_{120_i} - h_{60_i}}{h_{120_i}}\right| \tag{4-1}$$

Capillary pressure MARE between the coarser mathematical grid (60x60 elements) and the finer numerical grid (120x120 elements), for each infiltration rate and five of the Gaussian realizations are shown in Table **4-1**. As it can be seen in the table, all errors are lower than 1.2% which means that mathematical grids of 60x60 elements capture accurately capillary pressures and therefore flux through finite volume faces, this behavior is the same for all the realizations.

Table 4-1.: Capillary pressure MARE between results obtained with mathematical grids of 120x120 and 60x60 elements for the first five realizations of Gaussian fields.

Realization	Stationary Mean Pressure Head (m)			
	h=-20	h=-10	h=-5	h=-1
1	0.06	0.11	0.25	1.03
2	0.06	0.10	0.20	0.97
3	0.05	0.10	0.23	1.06
4	0.06	0.12	0.25	1.08
5	0.06	0.14	0.28	1.08

4.2. Numerical simulation of coarser hydraulic conductivity fields

Once known that a mathematical grid of 60x60 elements capture all desired effects and therefore generates "real results", numerical non-saturated infiltration simulations were performed maintaining the same initial and boundary conditions. Influence of hydraulic conductivity field element size, p and infiltration rate in capillary pressure and flux through finite volume faces (from now on called flux) was evaluated. Main behaviors are shown below.

4.2.1. Grid refinement level influence

For each one of the hydraulic conductivity field elements sizes (from now on called HCFES) and realization, the capillary pressure solution fields were compared with the real solution of the problem through the MARE calculation across the domain volumes; this is shown in Figure **4-1** for p=-1 and h=-20m. In there, capillary pressure MARE is plotted against the HCFES for each one of the realizations (gray lines); additionally, the average of their MARE is plotted (red line). As expected, capillary pressure MARE is higher for coarser hydraulic conductivity fields. Besides, dispersion of the data is higher for coarser hydraulic conductivity fields. The latest can be seen better in Figure **4-2**, where, instead of each one of the realizations relative error; the mean, the median, and a box plot of those errors are plotted for the same p and infiltration rate.

Despite previous behavior being the same for any p value and infiltration rate, some differences are revealed when p and the infiltration rate change. For instance, Figure **4-3** shows for p=-0.5 and h=-1m an important increase of the capillary pressure MARE (in comparison

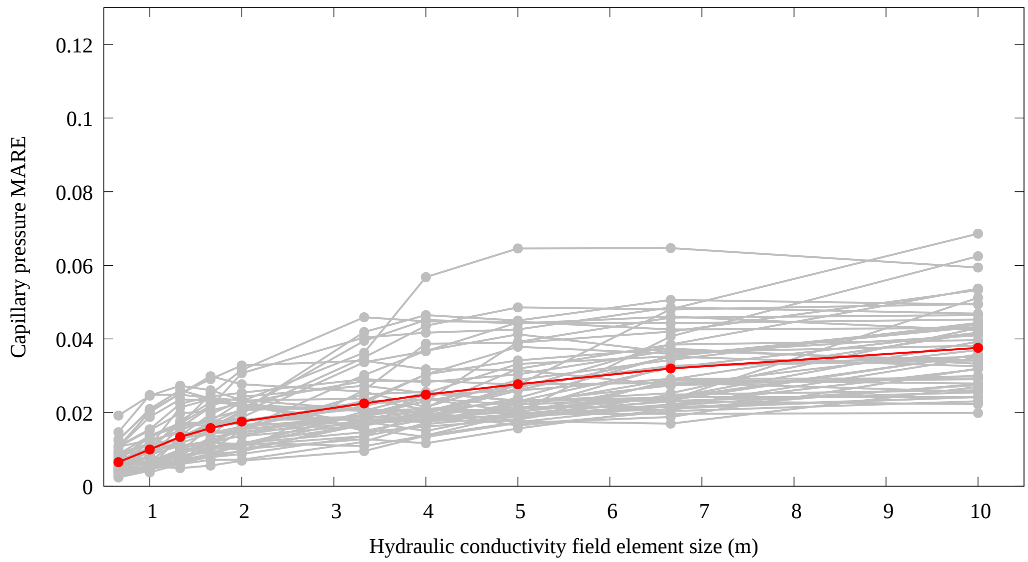

Figure 4-1.: Capillary pressure MARE against HCFES for p=-1 and h=-20m. Gray lines represent each one of the realizations and red line represents the average error of the realizations.

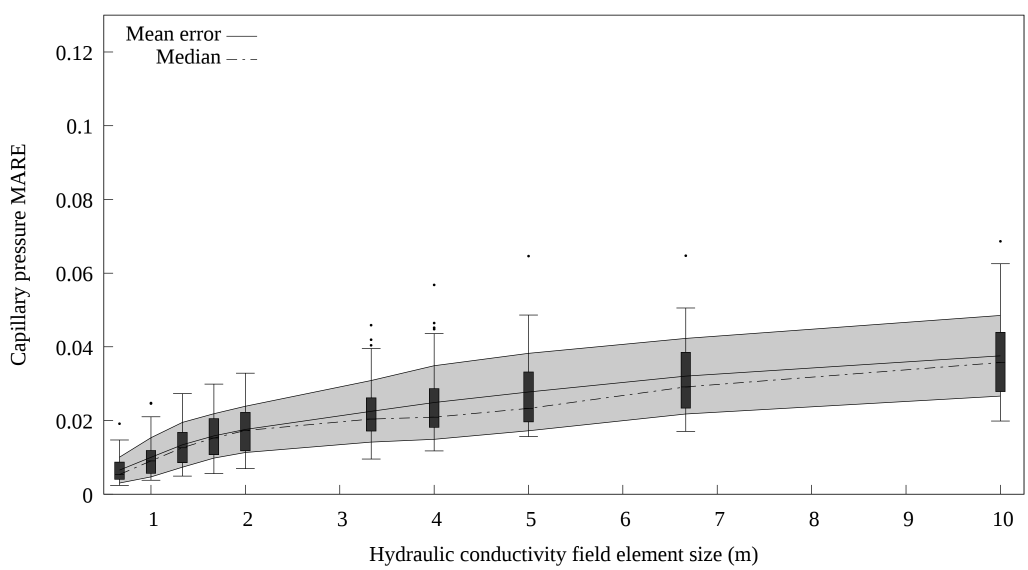

Figure 4-2.: Capillary pressure MARE statistics against HCFES for p=-1 and h=-20m.

with $p = -1$ and $h = -20m$).

Also, for any p and infiltration rate simulated, the median is equal or greater than the mean, this behavior is more evident for greater capillary pressures, which could imply that relative error of the solution is more sensible for lower infiltration rates or could be an effect obtained by lack of realizations. However, this should be investigated with a formal sensibility analysis.

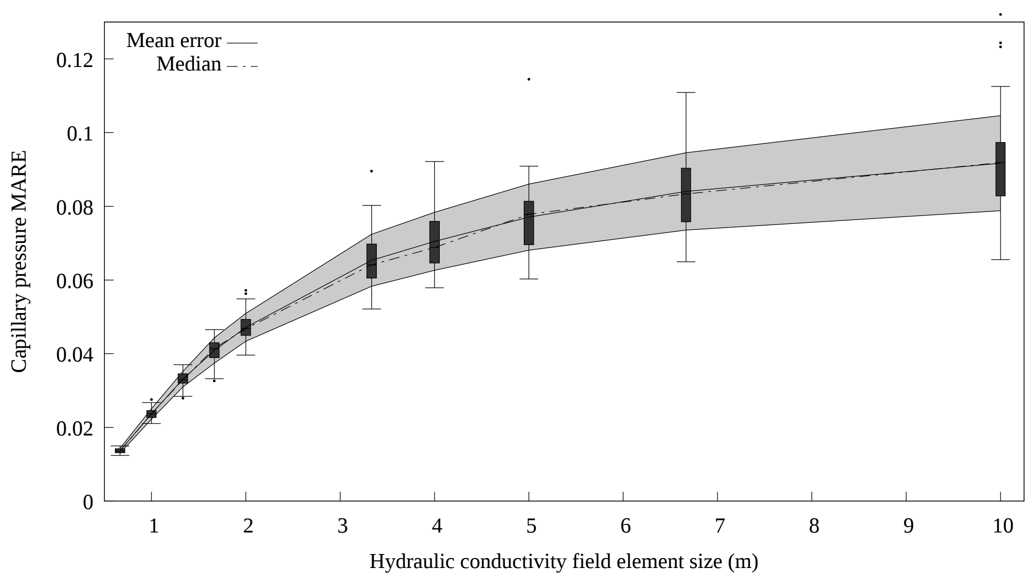

Figure 4-3.: Capillary pressure MARE against HCFES for p=-0.5 and h=-1m.

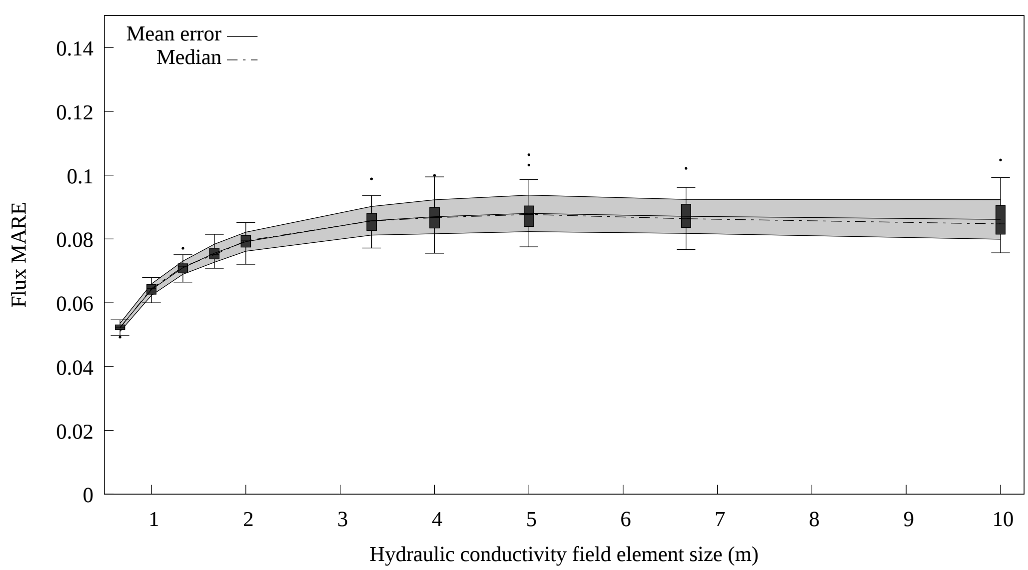

Figure 4-4.: Flux MARE against HCFES for p=-0.5 and h=-1m.

The bigger the HCFES, the greater the discrepancy between the fluxes obtained with a hydraulic conductivity upscaled field and the real fluxes, as it was expected. Also, for flux MARE the bigger the HCFES, the bigger the dispersion of the data. Figure **4-4** shows the flux MARE against HCFES for p=-0.5 and h=-1. If the previous Figure is compared with Figure **4-5** (p=-1 and h=-10) it can be seen an important change in the flux MARE changing p and infiltration rate.

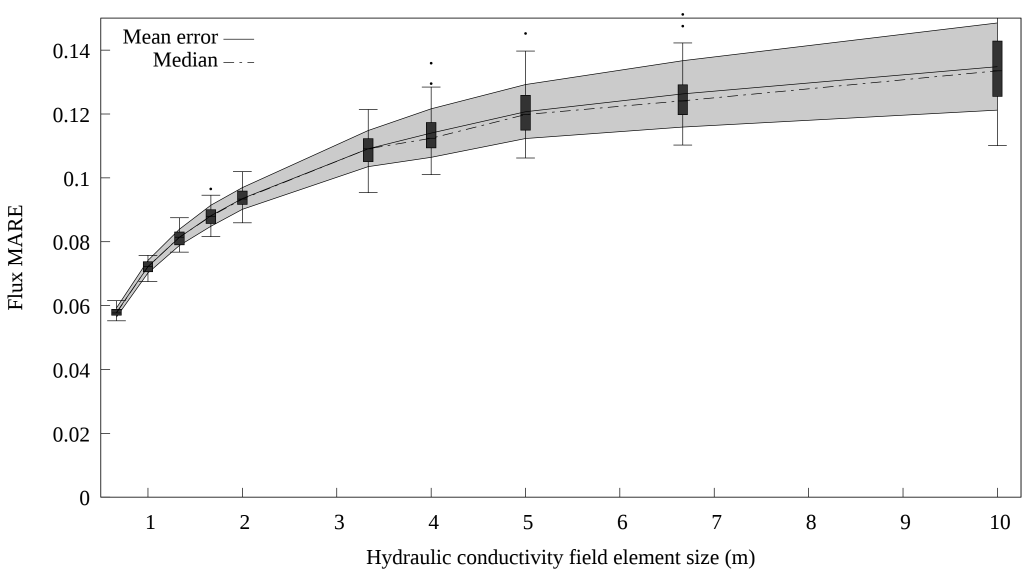

Figure 4-5.: Flux MARE against HCFES for p=-1 and h=-10m.

In figure **4-4**, flux MARE reaches a maximum close to HCFES=4 and then remains relatively constant. This implies that no matter the HCFES selected, flux MARE is asymptotic. In fact, in all the obtained plots (flux MARE and capillary pressure MARE), an incipient asymptotic behavior is evidenced when HCFES grow. Nevertheless, this behavior should be analyzed with bigger physical domains.

4.2.2. P-power influence

As shown in the previous section, capillary pressure MARE and flux MARE were influenced by the HCFES. However, this was not the unique parameter affecting the problem solution. The p upscaling parameter was also modified resulting in changes in the capillary pressure MARE (at least for Gaussian fields).

The latest affirmation rise by the comparison between Figures **4-2** and **4-3**, in there, it can be seen differences of the errors for all HCFES. When plotting capillary pressure MARE against p for some HCFE and h=-1m (Figure **4-6**), it appears to exist a minimum capillary pressure MARE for all the HCFES. Capillary pressure MARE has a minimum close to -0.5 of the p-power parameter (between harmonic and geometric mean). Capillary pressure MARE is greater in magnitude for coarser hydraulic conductivity fields; however, ratios between capillary pressure MARE at p=1 and p=-0.5 remains almost constant for different HCFES. This is, for h=-1, if hydraulic conductivity field is upscaled from 60x60 elements to 2x2 elements the capillary pressure MARE for p=1 is 10.59% and for p=-0.5 is 9.33% (difference of 1.26% and ratio of 1.14) and, if hydraulic conductivity field is upscaled from 60x60 elements to 30x30 elements the MARE for $p-power = 1$ is 1.71% and for $p-power = -0.5$ is 1.39%, (difference of 0.32% and ratio of 1.23).

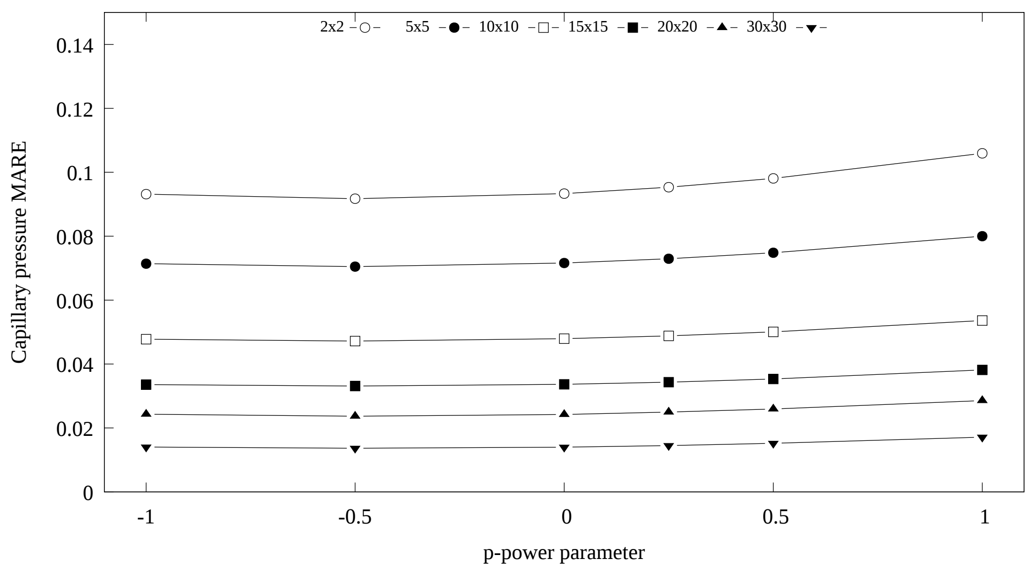

Figure 4-6.: Capillary Pressure MARE against p and h=-1m for some HCFES.

These findings suggested that when Gaussian hydraulic conductivity fields (or permeability fields) are upscaled using the generalized mean equation, p parameter selection is important to compute acceptable capillary pressure values. An optimal choice could reduce the capillary pressure MARE almost to half. In the case of non-saturated infiltration problems with a steady-state mean capillary pressure of $h = -1$, the optimal p according to the results of this work is a value closer to -0.5. However, the importance of this parameter and its optimal value also depends on the infiltration rate, as it can be seen in the next section.

p has not any significant influence in flux MARE. For Gaussian hydraulic conductivity fields, any infiltration rate and any refinement level the flux MARE remains almost constant for all p values considered in this work. This can be seen in Figure **4-7**, where flux MARE is plotted against p parameter for some HCFES and $h = -20m$. In the plot, it can not be seen any considerable variation of the flux MARE for any of the grid refinement levels nor any value of the p parameter, This behavior occurs for any infiltration rate. It is important to underscore that even if the variation is not significant (maximum ratio of flux MARE at p=1 and p=-0.5 equal to 1.01), optimum p (the one that produces smallest discrepancies between upscaled and finer fields) are the same that those obtained in the capillary pressure analysis.

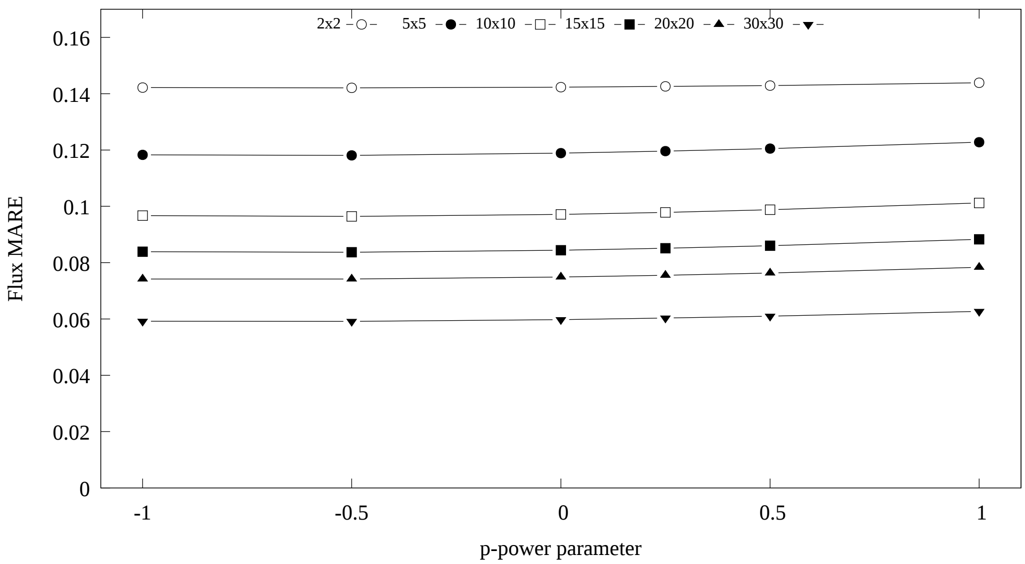

Figure 4-7.: Flux MARE against p parameter for $h = -20m$ and some of the HCFES.

4.2.3. Infiltration rate influence

Infiltration rate is another parameter to take into account when hydraulic conductivity fields are upscaled. According to this work results, lower infiltration rates produce smaller capillary pressure MARE. In general, for h=-20m and the coarser the grid, the capillary pressure MARE never exceeds 6.6% (with a minimum of 3.3%). On the other hand, for h=-1m and the same refinement level, capillary pressure MARE reaches values up to 10.6% (with a minimum of 9.3%), this for scaling from 60x60 elements to 2x2 elements. The behavior of MARE for different values of the $p-power$ upscaling parameter, different infiltration rates and upscaling from 60x60 to 2x2 elements is shown in Figure **4-8**. Where, capillary pressure MARE for h=-1m is always above than capillary pressure MARE for h=-5m, h=-10m and h=-20m.

Mentioned behavior is the same for all upscaling levels, however, starting in upscaling level from 60x60 to 10x10 elements, the difference between lower infiltration rates disappears (Figure **4-9**). This means that for Gaussian fields, infiltration rate influences the capillary

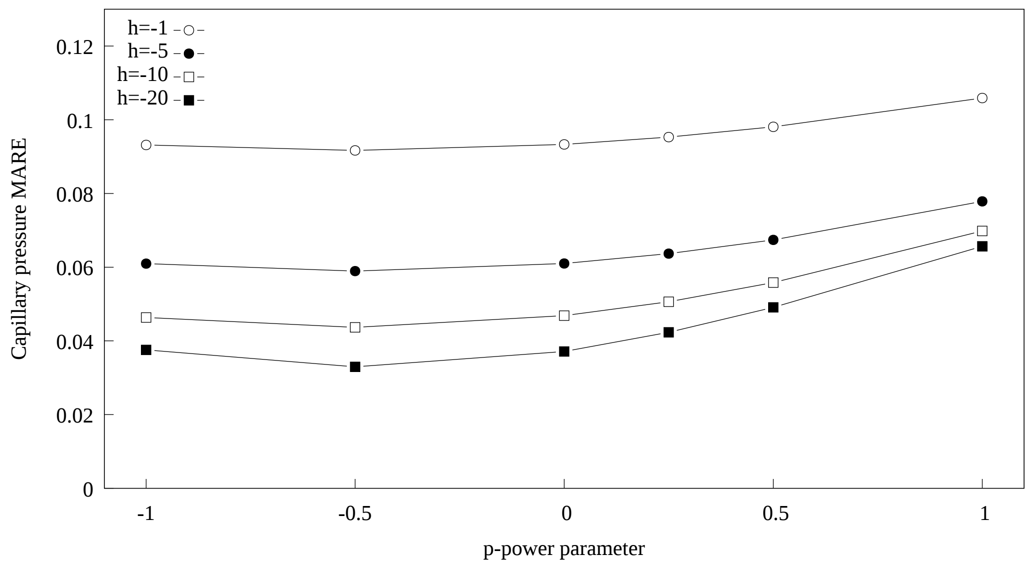

Figure 4-8.: Capillary pressure MARE against p for different infiltration rates and the bigger refinement level.

pressure MARE obtained when hydraulic conductivity fields are upscaled. However, for lower infiltration rates this influence disappears if the refinement level is small. i.e., if the change of the HCFES is small, the MARE is equal for lower infiltration rates (h=-5m, h=-10m and h=-20m). For this case, an increase factor of 6 in HCFES is the breaking point between infiltration rate dependence and independence.

Infiltration rate also influences the flux MARE. In general, simulations with higher infiltration rates produce lower flux MARE. In Figure **4-10** flux MARE is plotted against p for different infiltration rates and an upscaling from 60x60 to 30x30 hydraulic conductivity elements. In there, it can be seen that higher flux MARE corresponds to the lower infiltration rate and vice versa. In the Figure, it is evident a variation of the error in function of p as well; however, this influence is not relevant.

The last section showed that p upscaling parameter influences the upscaling of Gaussian hydraulic conductivity fields. However, it depends on the infiltration rate according to the results of this work, in other words, for lower infiltration rates, p has more influence in capillary pressure MARE.

Figure **4-11** shows the capillary pressure MARE against p parameter for some HCFES and all studied infiltration rates. According to this Figure, capillary pressure MARE is higher for higher infiltration rates; also, the p parameter has more influence for lower infiltration rates. In the Figure, it is possible to see that starting at some point between h=-5m and

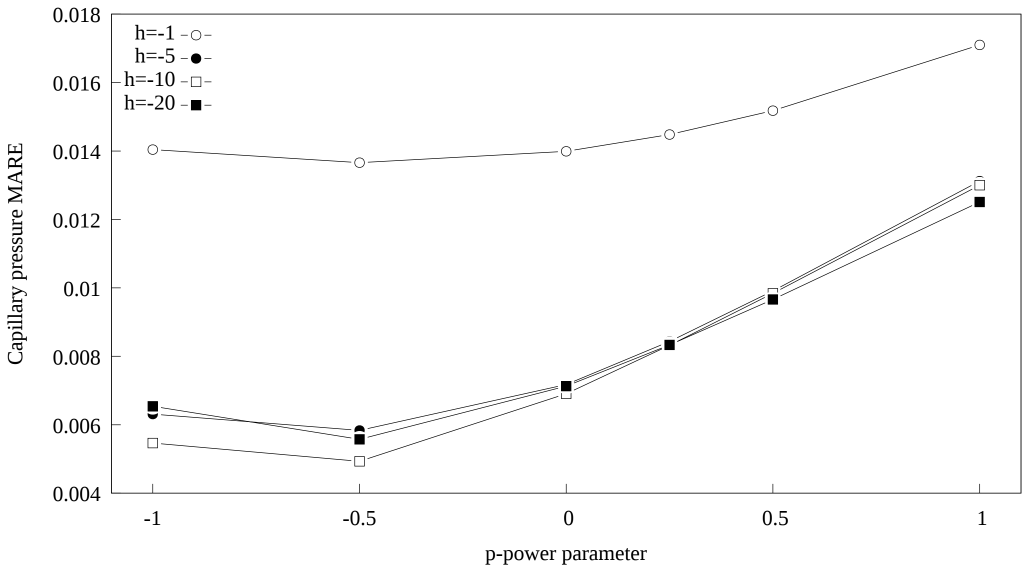

Figure 4-9.: Capillary pressure MARE against p for different infiltration rates and the smaller grid refinement level.

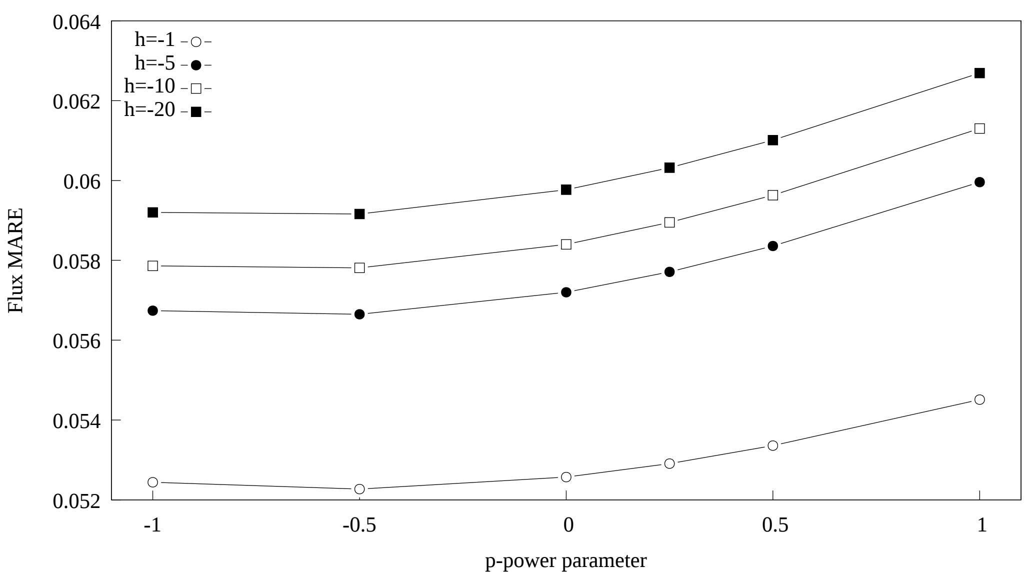

Figure 4-10.: Flux MARE against p for different infiltration rates and the smaller grid refinement level.

h=-10m capillary pressure MARE is independent of infiltration rate.

It appears that variation of the MARE is almost inexistent for the smaller grid refinement levels. However, computing ratios between capillary pressure MARE at p=-0.5 and p=1, the influence of p for different infiltration rates is presented in Table **4-2**.

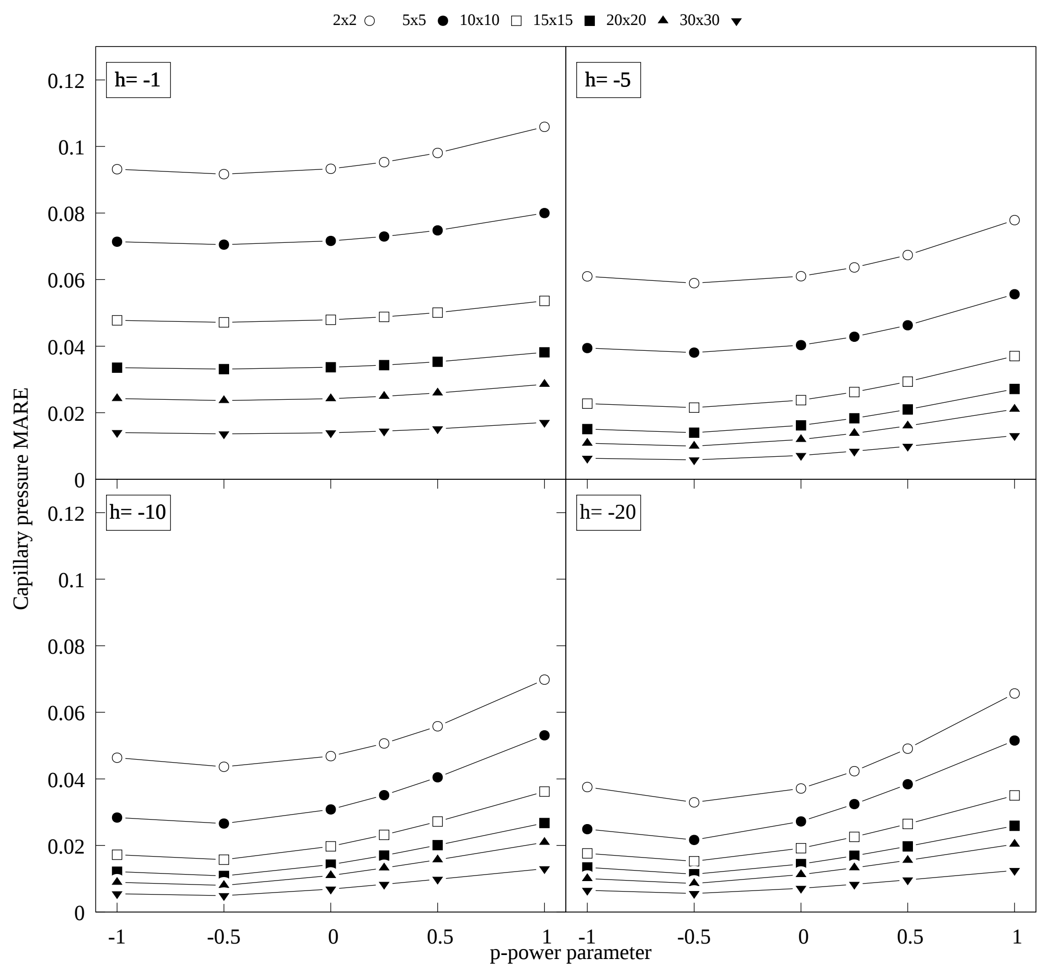

Figure 4-11.: Capillary pressure MARE against p for some HCFES and all infiltration rates.

Table 4-2.: Ratio between MARE at p=-0.5 and MARE at p=1 for some HCFES and different infiltration rates.

H.C. grid	Mean capillary pressure			
	h=-20m	h=-10m	h=-5m	h=-1m

2x2	0.50	0.63	0.76	0.87
5x5	0.42	0.50	0.68	0.88
15x15	0.44	0.41	0.52	0.87
30x30	0.45	0.38	0.45	0.80

In general, the ratio between capillary pressure MARE at $p = -0.5$ and $p = 1$ decreases with the HCFES and with the infiltration rate. Then, for higher infiltration rates, the ratio is higher, indicating that the difference between both capillary pressure MARE is smaller. i.e., for higher infiltration rates the diminution of error is smaller for the optimal p. Last behavior can also be seen with the absolute difference between both capillary pressure MARE (Table **4-3**).

Figure **4-12** was plotted to correctly understand flux MARE as a function of the infiltration rate. No matter the value of infiltration rate, flux MARE is practically independent of p. Besides, starting at some point between h=-5m and h=-10m, the variation of the flux MARE is independent of infiltration rate.

Table 4-3.: Difference between MARE obtained with $p{-}power = -0.5$ and MARE obtained with $p - power = 1$ for different hydraulic conductivity grids and different infiltration rates.

H.C. grid	Mean capillary pressure			
	h=-20m	h=-10m	h=-5m	h=-1m
2x2	3.27%	2.62%	1.89%	1.42%
5x5	2.99%	2.65%	1.76%	0.95%
15x15	1.45%	1.59%	1.31%	0.50%
30x30	0.69%	0.81%	0.73%	0.34%

In Table **4-3**, capillary pressure MARE difference is higher for lower infiltration rates and bigger HCFES. According to this table, in problems with high infiltration rates, selection of an optimal p is not as important as it is for problems with lower infiltration rates. Nevertheless, it exists an optimal p in the range [-0.5,0] being closer to 0 for higher infiltration rates and closer to -0.5 for lower infiltration rates.

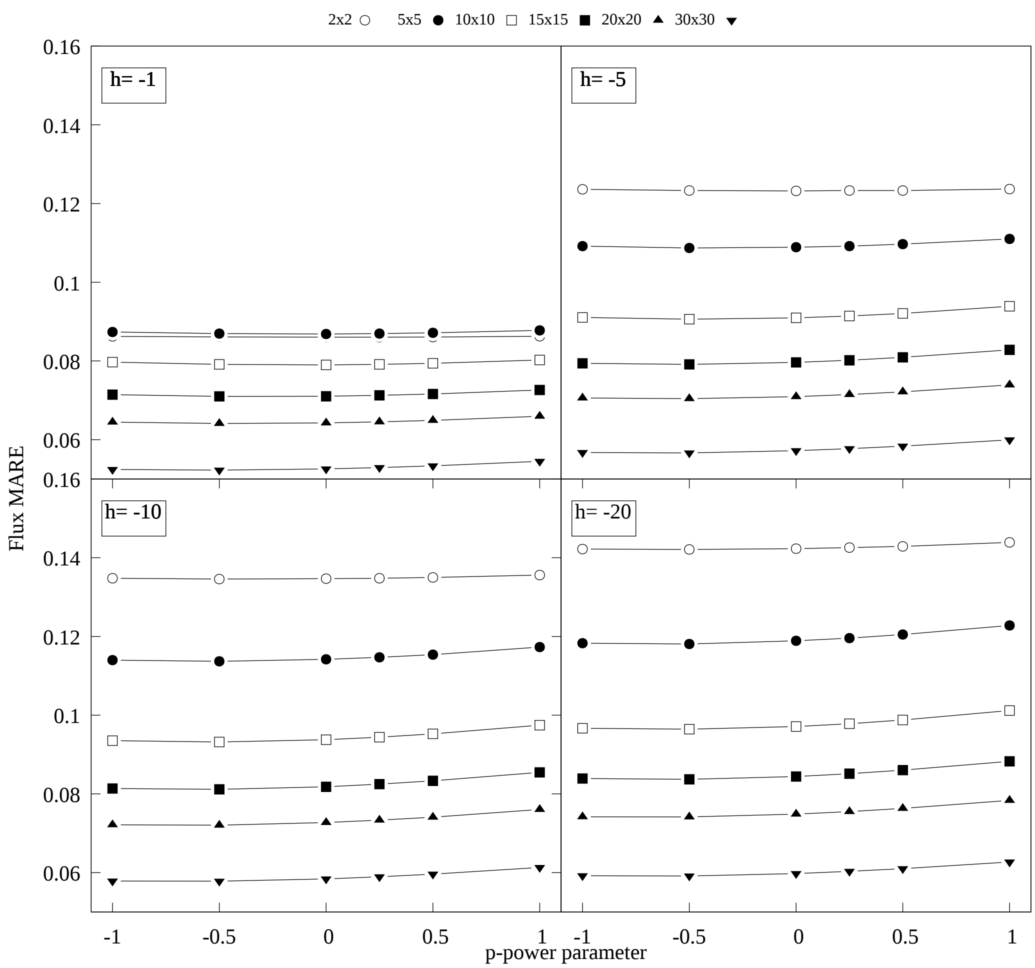

Figure 4-12.: Flux MARE against p for some HCFES and all infiltration rates.

This chapter has shown for Gaussian fields: a mesh independence test and the key points found when simulation results with upscaled hydraulic conductivity fields and real results are compared. Next chapter will show a similar discussion, but for non-Gaussian fields, also, it will show the major differences in the numerical flow simulation and upscaling when non-Gaussian fields are used.

5. Numerical Implementation and Results - non-Gaussian Fields

The previous chapter showed results and a discussion about flow numerical simulations performed with Gaussian fields. This chapter will show a similar analysis but about the results of non-Gaussian fields. Additionally, main differences between Gaussian and non-Gaussian results will be shown and discussed.

5.1. Mesh independence test

It was performed a mesh independence test similar to the one used for the Gaussian fields. Capillary pressure MARE between the coarser mathematical grid (60x60 elements) and the finer mathematical grid (120x120 elements) for each infiltration rate and five of the non-Gaussian realizations are shown in Table **5-1**. Similar behavior occurs for the other realizations.

Table 5-1.: Capillary pressure MARE (%) between 120x120 and 60x60 mathematical grids for the first five realizations of non-Gaussian fields

Realization	Stationary Mean Pressure Head (m)			
	h=-20	h=-10	h=-5	h=-1
1	0.06	0.11	0.25	1.03
2	0.06	0.10	0.20	0.97
3	0.05	0.10	0.23	1.06
4	0.06	0.12	0.25	1.08
5	0.06	0.14	0.28	1.08

As it can be seen in the table, all errors are lower than 2% which means that mathematical grids of 60x60 elements capture accurately capillary pressures and therefore flux through finite volume faces, this behavior is the same for all realizations and all non-Gaussian hydraulic conductivity fields studied in this work.

In addition, for all Gaussian and non-Gaussian fields, mesh independence test gives better results (smaller capillary pressure differences between grids) for lower infiltration rates. Furthermore, capillary pressure MARE gets lower with smaller values of the α simulation parameter of the non-Gaussian fields; however, this drop stops for non-Gaussian fields of $\alpha = 1.5$.

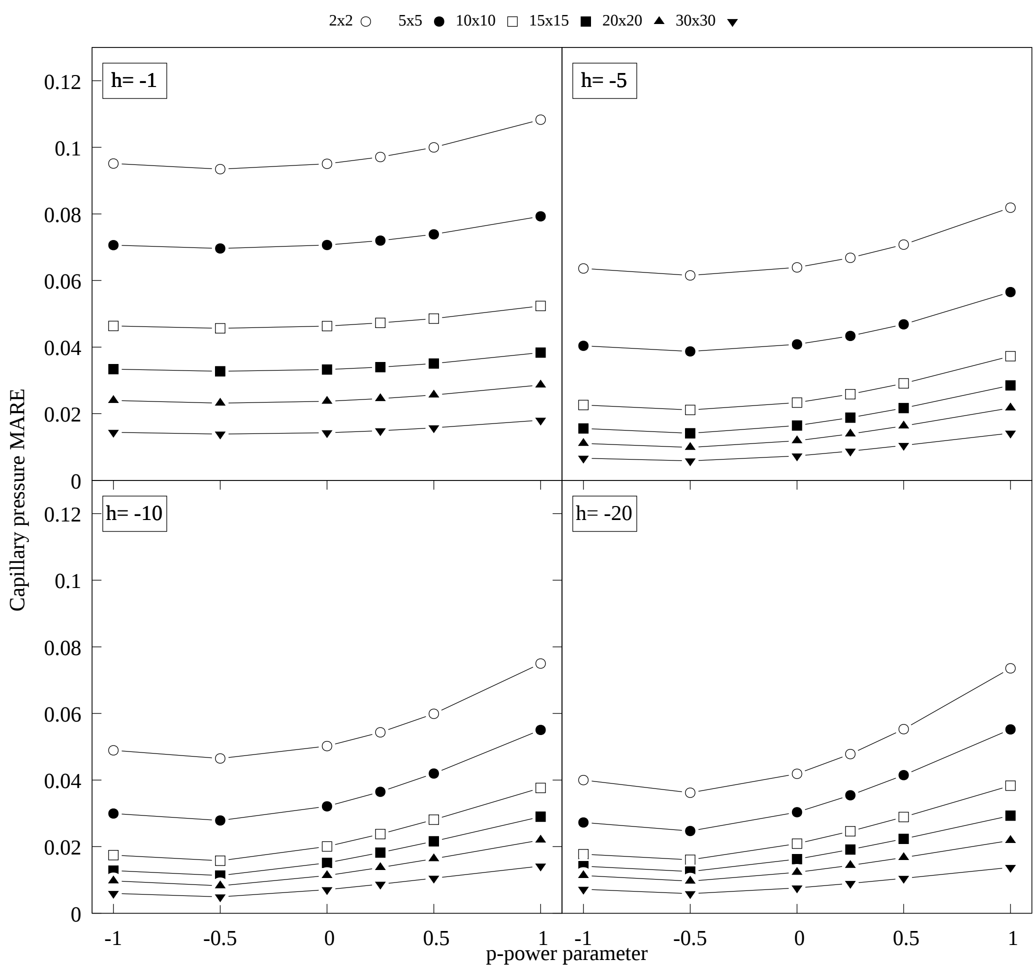

Figure 5-1.: Capillary pressure MARE for non-Gaussian fields (α=1.8).

5.2. Numerical simulation of coarser hydraulic conductivity fields

Once performed the mesh independence test, numerical simulations of non-saturated infiltration were performed maintaining the same initial and boundary conditions but with upscaled hydraulic conductivity fields. Influence of non-Gaussianity, grid refinement level, p upscaling parameter and infiltration rate in capillary pressures and flux was evaluated.

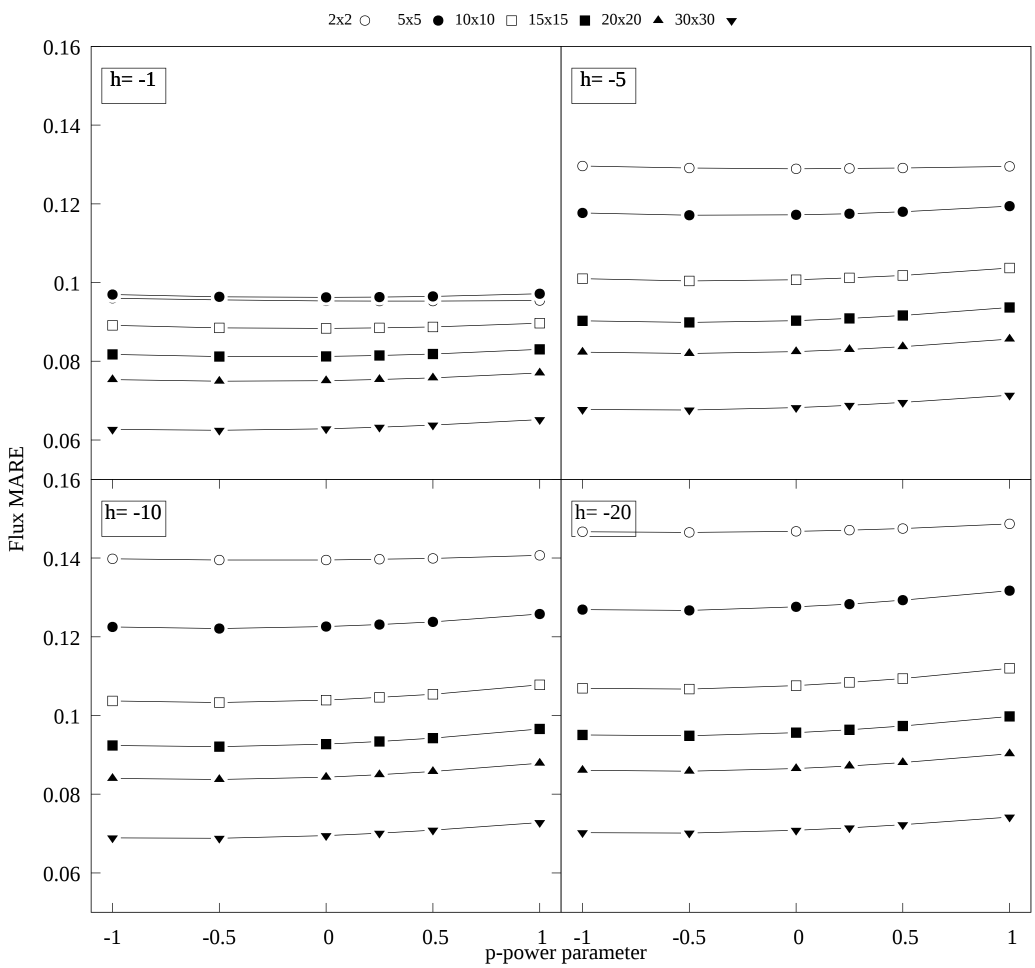

Figure 5-2.: Flux MARE for non-Gaussian fields (α=1.8).

5.2.1. Grid refinement level

For each HCFES and realization, capillary pressure solutions obtained with upscaled fields were compared with the real solution of the problem (capillary pressure solution obtained with a 60x60 elements field) through the MARE calculation across the domain volumes. As expected, capillary pressure MARE is higher for coarser hydraulic conductivity fields. The latest can be seen in Figure **5-1**, there, capillary pressure MARE is higher for higher HCFES for any infiltration rate and any p. Similar behavior was found for flux MARE (Figure **5-2**).

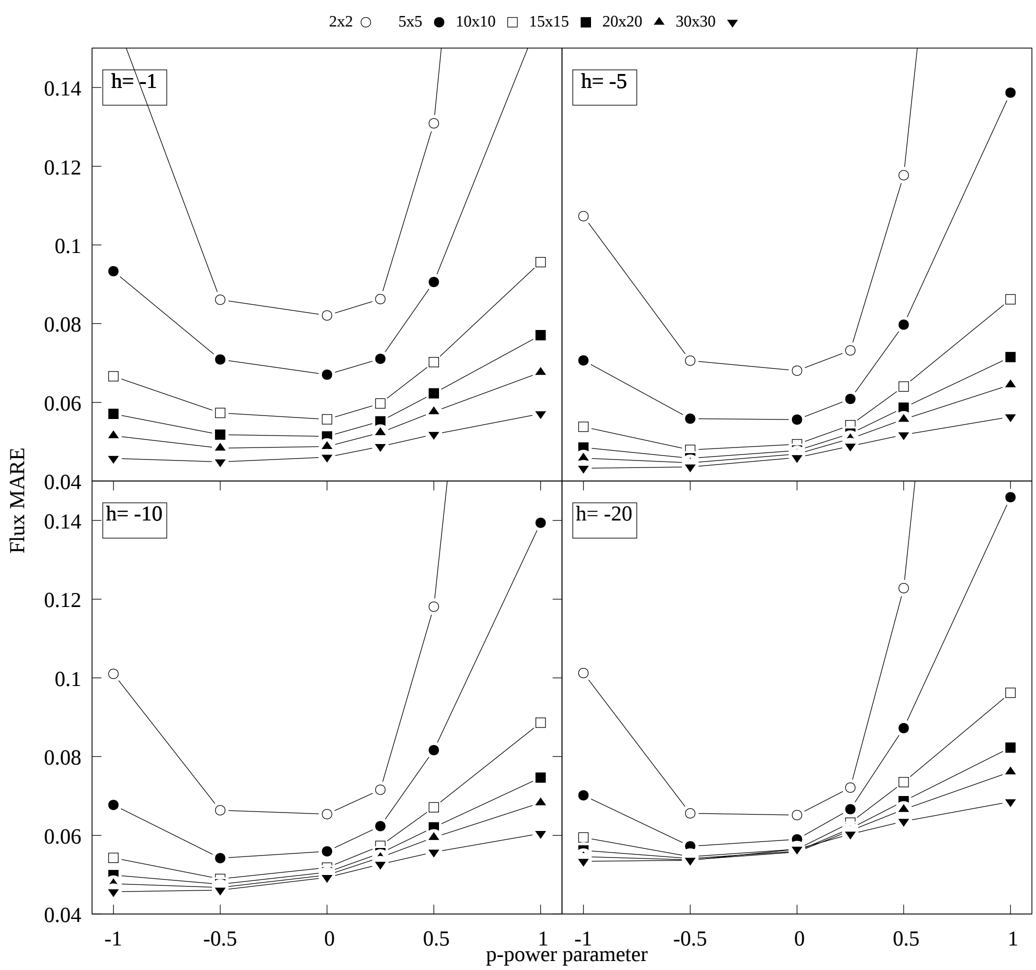

Figure 5-3.: Capillary pressure MARE for non-Gaussian fields (α=1.2).

5.2.2. p-power influence

$p-$power influences capillary pressure MARE but not in flux MARE for non-Gaussian fields with α non-Gaussianity parameter closer to 2. However, a slightly bigger influence starts to appear in both flux and capillary pressure MARE when α decreases. The smaller the α non-Gaussianity parameter the bigger the influence of p (Figures **5-1**, **5-2**, **5-3** and **5-4**).

Similar plots but for other α values are shown in Appendix B.

It is important to point out that the optimum value of p changes with α: the optimum p starts to be closer to -1 if α decreases, i.e., if the field is less Gaussian.

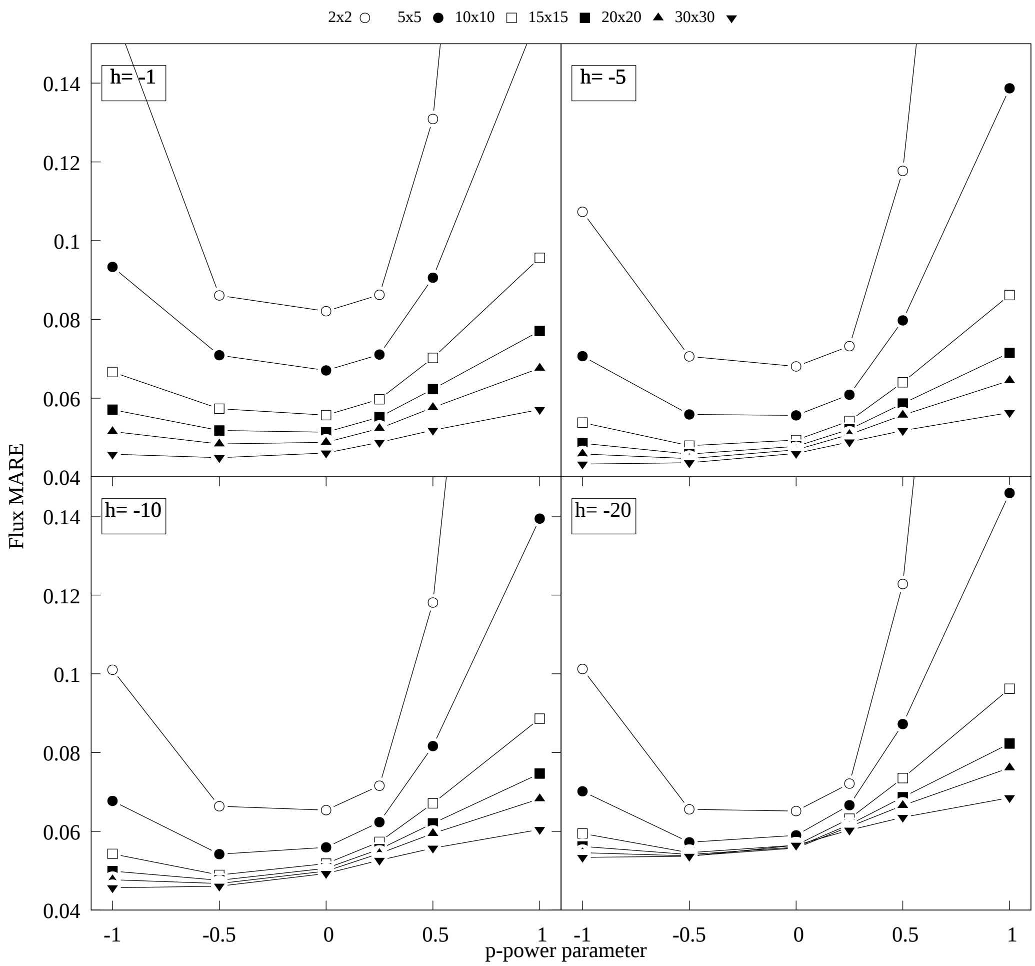

Figure 5-4.: Flux MARE for non-Gaussian fields (α=1.2).

5.2.3. Infiltration rate influence

Infiltration rate has a clear influence in flux and capillary pressure MARE (Figures **5-3** and **5-4**). Capillary pressure MARE increases and flux MARE decreases with infiltration rate. However, it appears to exists a point between h=-5m and h=-10m below which capillary pressure and flux MARE will not be affected by infiltration rate.

5.2.4. Comparison between Gaussian and non-Gaussian fields

When flux and capillary pressure MARE produced by Gaussian and non-Gaussian fields are compared, it can be seen that in general, the smaller the α non-Gaussianity parameter, the bigger the capillary pressure and flux MARE at p extreme values. Besides, it is evident that the selection of optimum p gets more importance in non-Gaussian fields, in those, a wrong choice of p (e.g., arithmetic mean) could produce huge discrepancies between results obtained with fine and coarse grids. e.g., Capillary pressure MARE obtained with $p = -0.5$ produces similar plots for any type of fields, however, for $p = 1$ non-Gaussian fields have higher capillary pressure MARE (Figures **5-3** and **5-4**).

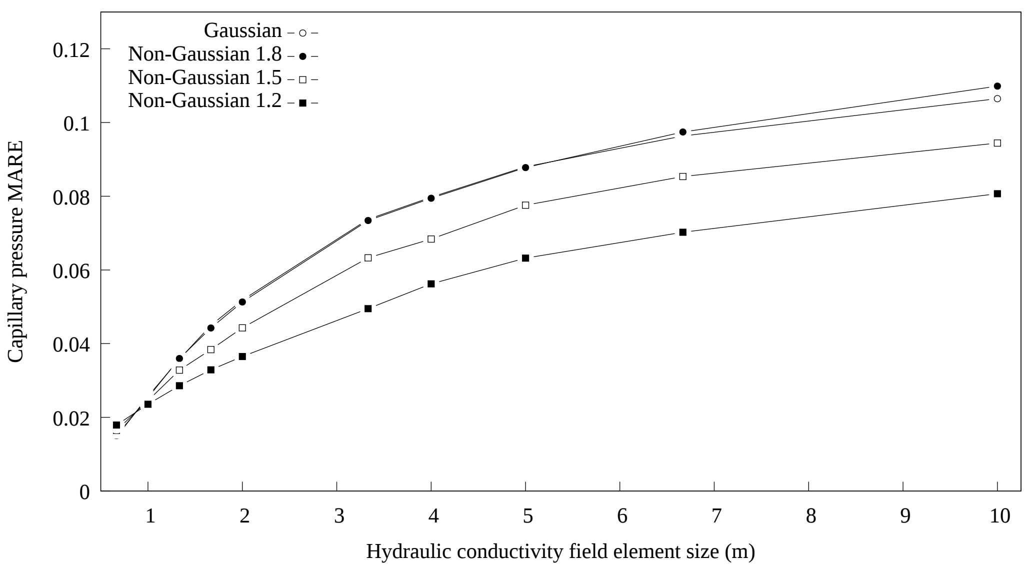

Figure 5-5.: Capillary pressure MARE against HCFES for p=0 and h=-1m.

Figure **5-5** shows capillary pressure MARE against HCFES for Gaussian and non-Gaussian fields, p=0 and h=$-$1m. According to those Figures the less Gaussian the field, the less capillary pressure MARE for any HCFES. However, it is important to underline that α non-Gaussianity parameter depends on the study case and it can be estimated with the methodologies proposed by Riva et al. (2015). Figure **5-6** shows log-capillary pressure MARE against HCFES for Gaussian and non-Gaussian fields, p=1 and h=$-$1m. Conforming to this Figure, the less Gaussian the field, the higher the capillary pressure MARE.

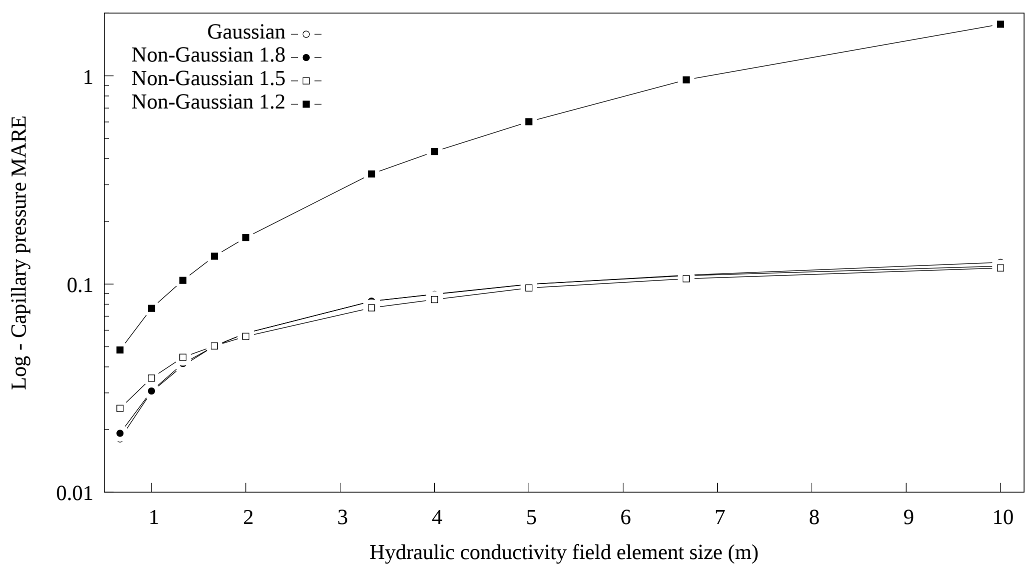

Figure 5-6.: log-capillary pressure MARE against HCFES for p=1 and $h = -1m$.

6. Summary, Conclusions and Recomendations

Influence of hydraulic conductivity field element size (HCFES), infiltration rate, $p-$power upscaling parameter and non-Gaussianity on hydraulic conductivity upscaling (from support volume to block scale) on a two-dimensional unsaturated infiltration numerical problem was evaluated. Analyses were framed in a probabilistic context, where hydraulic conductivity was conceptualized as a random space process. To achieve this, multiple realizations of hydraulic conductivity were performed and then infiltration problems were simulated varying each one of the mentioned parameters. Specifically, capillary pressure and vertical flux results were used to compare each one of the parameter combinations with the real solution of the problem (assumed to be the one performed with the finer hydraulic conductivity and mathematical grids). Some suppositions were required:

- Drying cycles were not taken into account during the simulations.
- Hysteresis was ignored.
- Stationarity in the mean was assumed.
- Ergodicity was assumed.
- It was not performed any experimental comparison.
- Comparisons were performed only for steady-state conditions.

Taking into account the aforementioned suppositions the following results were found.

As expected, one of the key parameters was the HCFES since the greater the HCFES, the bigger the discrepancy between the numerical simulations and the real solution of the problem (measured with a mean absolute relative error - MARE). The latest is a generalized behavior; it means that no matter the combination of the other parameters, this behavior was always the same.

Hydraulic conductivity field element size - HCFES influence in capillary pressure MARE and flux MARE was expected, this behavior could be attributed to the direct dependence between the solution and the field properties. In other words, even though the mathematical grid allowed 60x60 solutions, the property limits the solution of the problem within hydraulic conductivity field elements. This causes that the bigger the HCFES, the more finite volumes defined by the same property value. Besides, when hydraulic conductivity fields are upscaled, extreme values disappear making virtually impossible obtaining extreme values in the solution.

Varying $p-$power upscaling parameter, it was found that there exists a common optimum p for all HCFES. However, according to the results of this work, that value has slight differences for different infiltration rates being closer to 0 (geometric mean) for higher infiltration rates and closer to -0.5 for smaller infiltration rates. In addition, looking for smaller flux MARE, $p-$power upscaling parameter has not any significant influence when Gaussian fields are simulated; however, optimum $p-$power values are the same than those obtained for optimum capillary pressure MARE. On the other hand, it was found that p has an important influence on flux MARE when non-Gaussian fields are employed

Influence of $p-$power in the solution could be understood analyzing the generalized mean equation. This equation takes as input values of a variable and obtains an average using the $p-$power parameter. It could be demonstrated that the higher $p-$power, the closer the average to the maximum input and the smaller the $p-$power the closer the average to the minimum input. The generalized mean is a non-linear increasing function in the (-∞, + ∞) range, then, harmonic mean will always be smaller than geometric mean and geometric mean will be consistently lower than the arithmetic mean. The latest implies than when harmonic and arithmetic mean are used to upscale a hydraulic conductivity field, more extreme values are lost than when non-extreme values of $p-$power are used.

Infiltration rate also influences the numerical experiments performed. In general, for any type of field, Gaussian and non-Gaussian, the smaller the infiltration rate (and thereby the soil moisture), the lower the flux MARE and the higher the capillary pressure MARE. However, according to our results, there appears to exist a breaking point between infiltration rate dependence and independence between h=-5m and h=-10m in the capillary pressure MARE associated with the increasing factor of the HCFES. Also, it was found that the smaller the infiltration rate, the more important p selection is.

Capillary pressure and flux MARE independence of higher infiltration rates could be explained by the shape of the saturation function, in which, the variation of capillary pressure is smaller for higher values of capillary pressure. On the other hand, the fact that higher infiltration rates produce higher capillary pressure MARE could be better understood looking at particular solutions of the problems. There, the solution of the capillary pressure for $h=-20$m is smoother than for $h=-1$m. A smooth behavior is easier to represent even for a coarser grid; however, an erratic solution is harder to describe with the same mesh.

The fact that lower infiltration rates produce smoother solutions could be explained by the dimensional analysis of Darcy's law. On average, in fields with higher infiltration rates, flux through finite volume faces should be higher than in fields with lower infiltration rates (in this case a ratio $\approx 10^6$ between the highest and lowest infiltrations used). Additionally, hydraulic conductivity should be greater for higher infiltration rates (in this case a ratio $\approx 10^2$ between the highest and lowest infiltrations used). Therefore, hydraulic gradients between adjacent volumes should be on average higher for higher infiltration rates.

Non-Gaussianity of the fields shows an influence in the capillary pressure MARE, this is, α non-Gaussianity parameter values closer to 2.0 (Gaussian fields) produces bigger capillary pressure MARE for almost all the HCFES at optimum p values, however, at p equal to 1 or -1, non-Gaussian fields always give huge capillary pressure and flux MARE.

Finally, non-Gaussian capillary pressure MARE for $p-$power closer to 1.0 could be understood by the fact that in this work were generated fields of log-hydraulic conductivity. Those fields create then hydraulic conductivity distributions with more values above than below the mean, besides, due to the non-Gaussian assumption of the field some outstanding extreme values will be generated. With a field like the one described, when hydraulic conductivity is upscaled with an arithmetic average, big mistakes will be expected in elements where extreme values exist.

A. Appendix: Experimental and analytical covariance functions of the generated fields

This appendix contains plots of the theoretical and experimental covariance functions for Gaussian and sub-Gaussian fields.

A.1. Gaussian fields

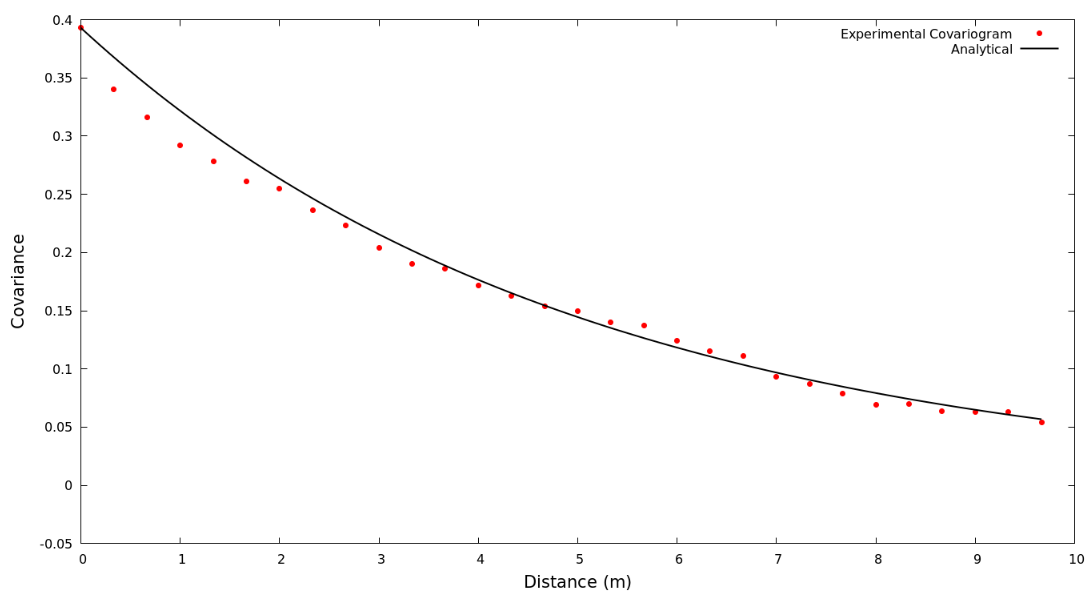

Figure A-1.: Experimental and analytical covariance function of the Gaussian fields in the X-direction

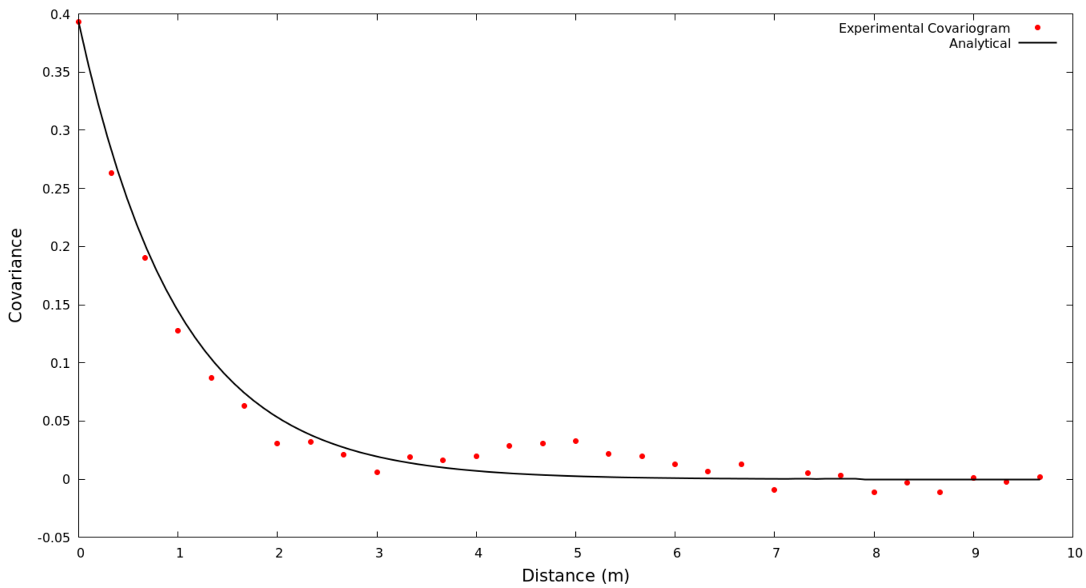

Figure A-2.: Experimental and analytical covariance function of the Gaussian fields in the Y-direction

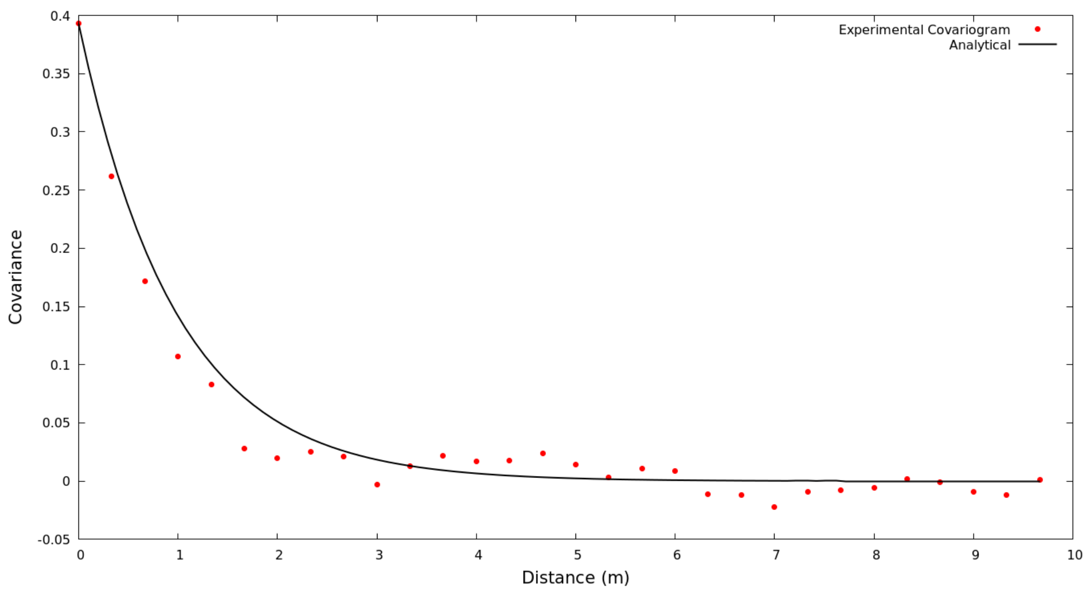

Figure A-3.: Experimental and analytical covariance function of the Gaussian fields in the $y = x$ direction

A.2. Non-Gaussian fields $\alpha = 1.8$

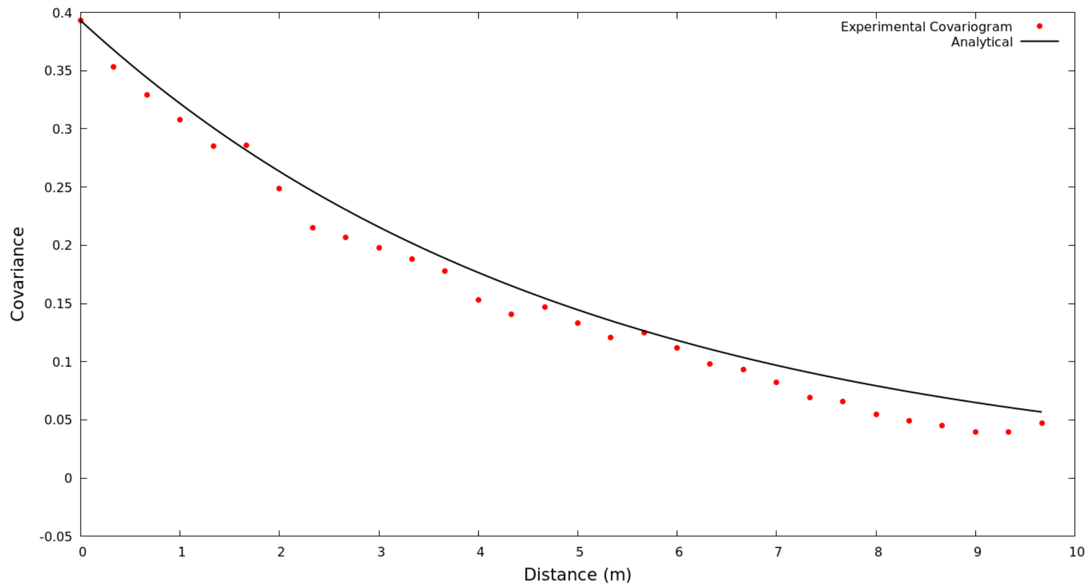

Figure A-4.: Experimental and analytical covariance function of the sub-Gaussian fields ($\alpha = 1.8$) in the x-direction

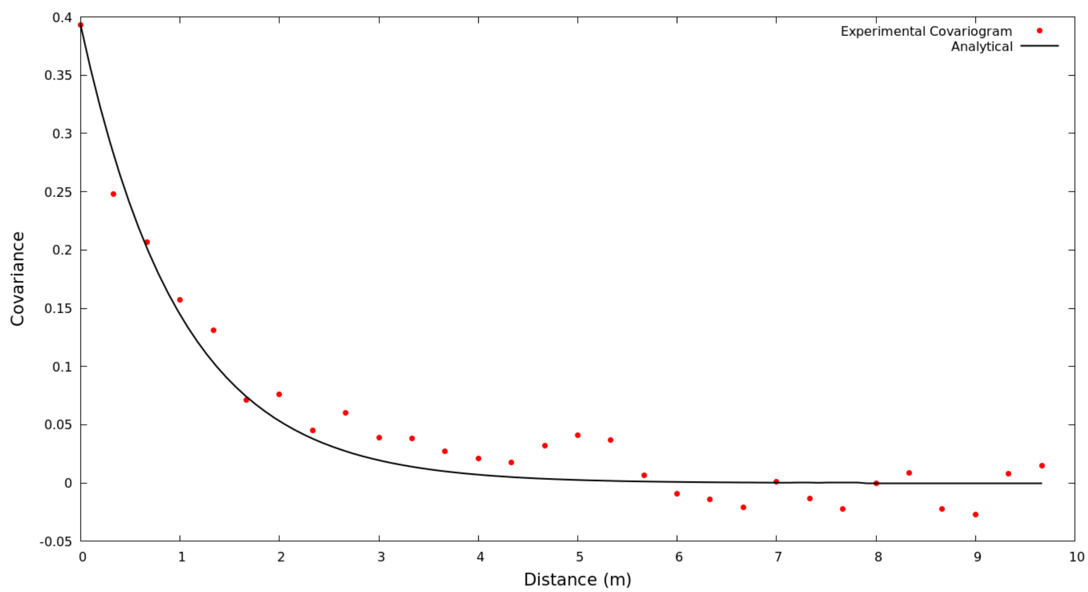

Figure A-5.: Experimental and analytical covariance function of the sub-Gaussian fields ($\alpha = 1.8$) in the y-direction

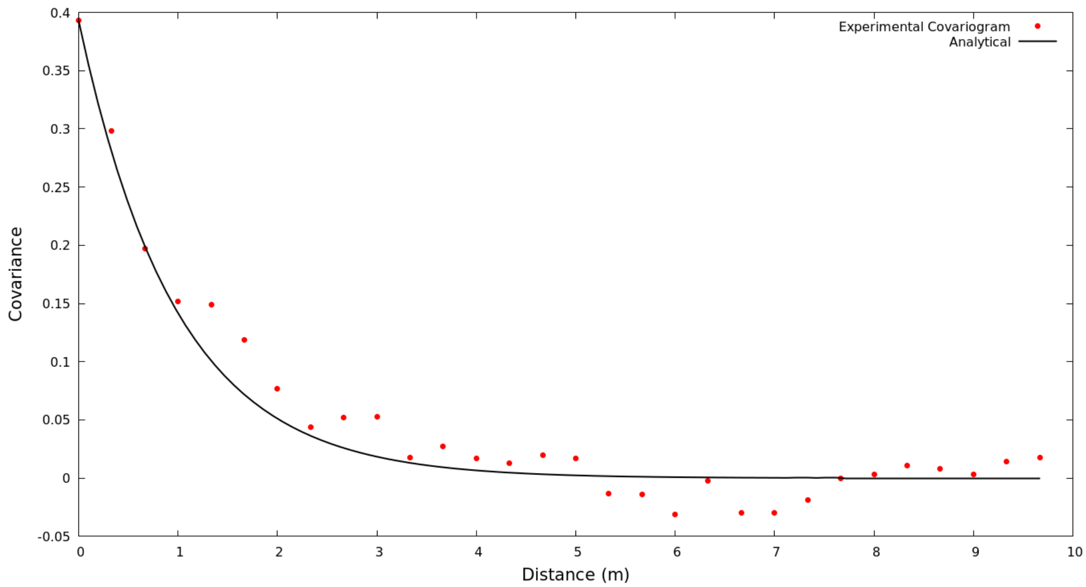

Figure A-6.: Experimental and analytical covariance function of the sub-Gaussian fields ($\alpha = 1.8$) in the $y = x$ direction

A.3. Non-Gaussian fields $\alpha = 1.5$

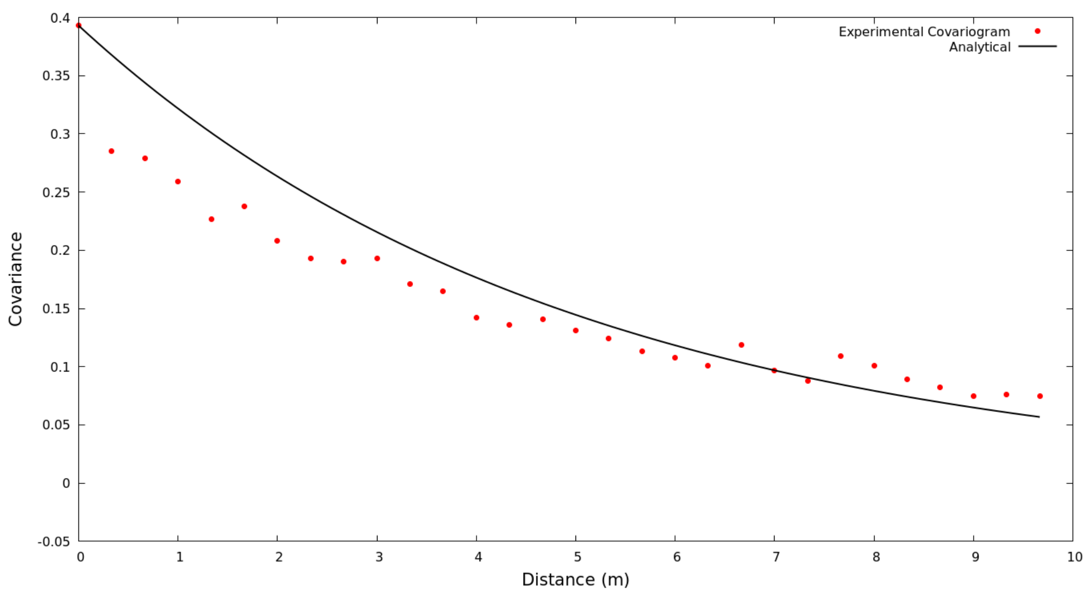

Figure A-7.: Experimental and analytical covariance function of the sub-Gaussian fields ($\alpha = 1.5$) in the x-direction

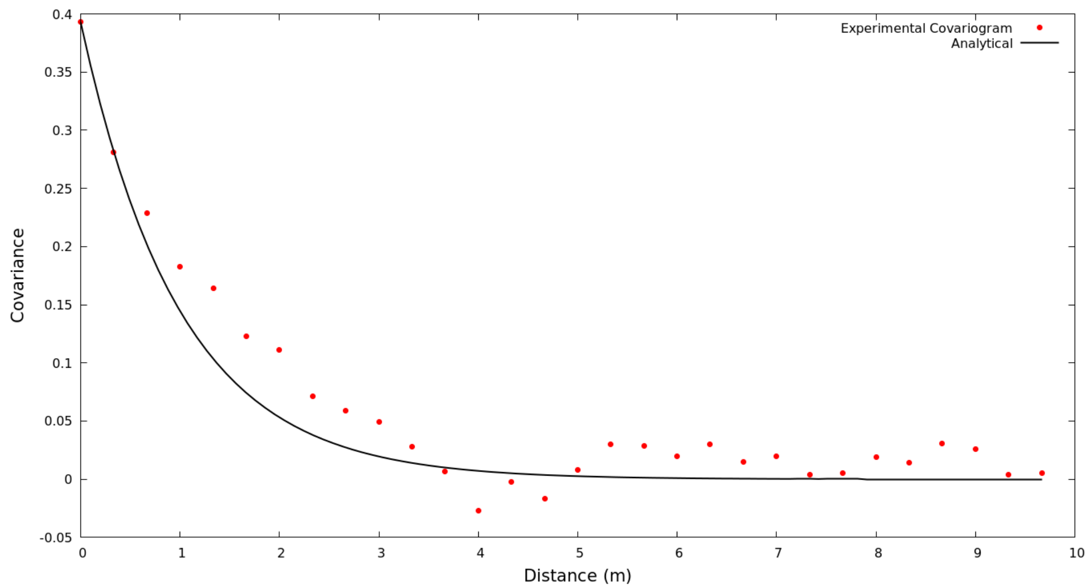

Figure A-8.: Experimental and analytical covariance function of the sub-Gaussian fields ($\alpha = 1.5$) in the y-direction

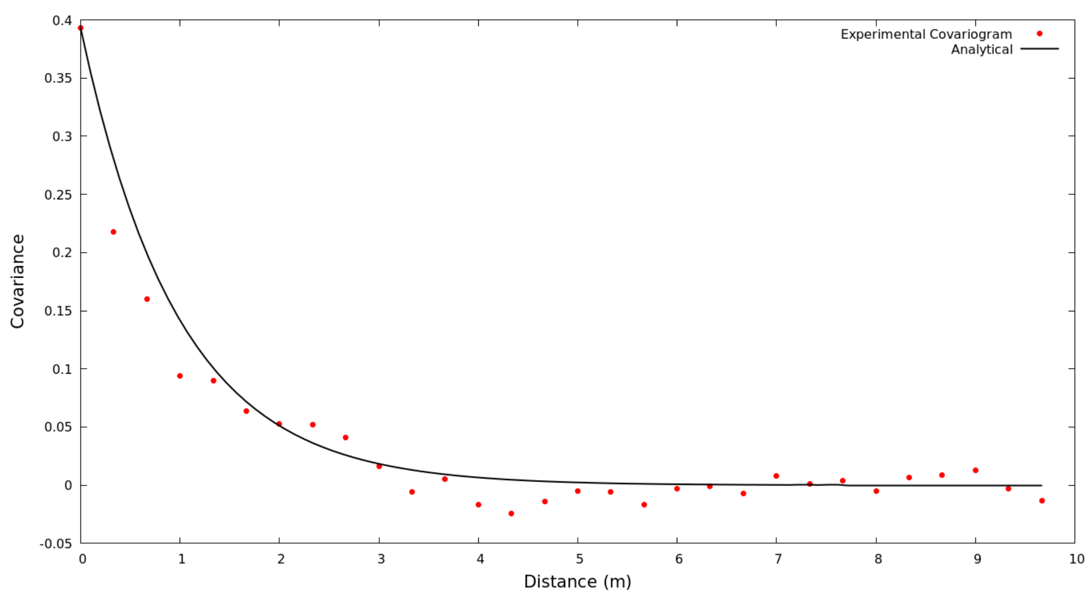

Figure A-9.: Experimental and analytical covariance function of the sub-Gaussian fields ($\alpha = 1.5$) in the $y = x$ direction

B. Appendix: Capillary pressure and flux MARE for non-Gaussian fields

B.1. Non-Gaussian fields α=1.9

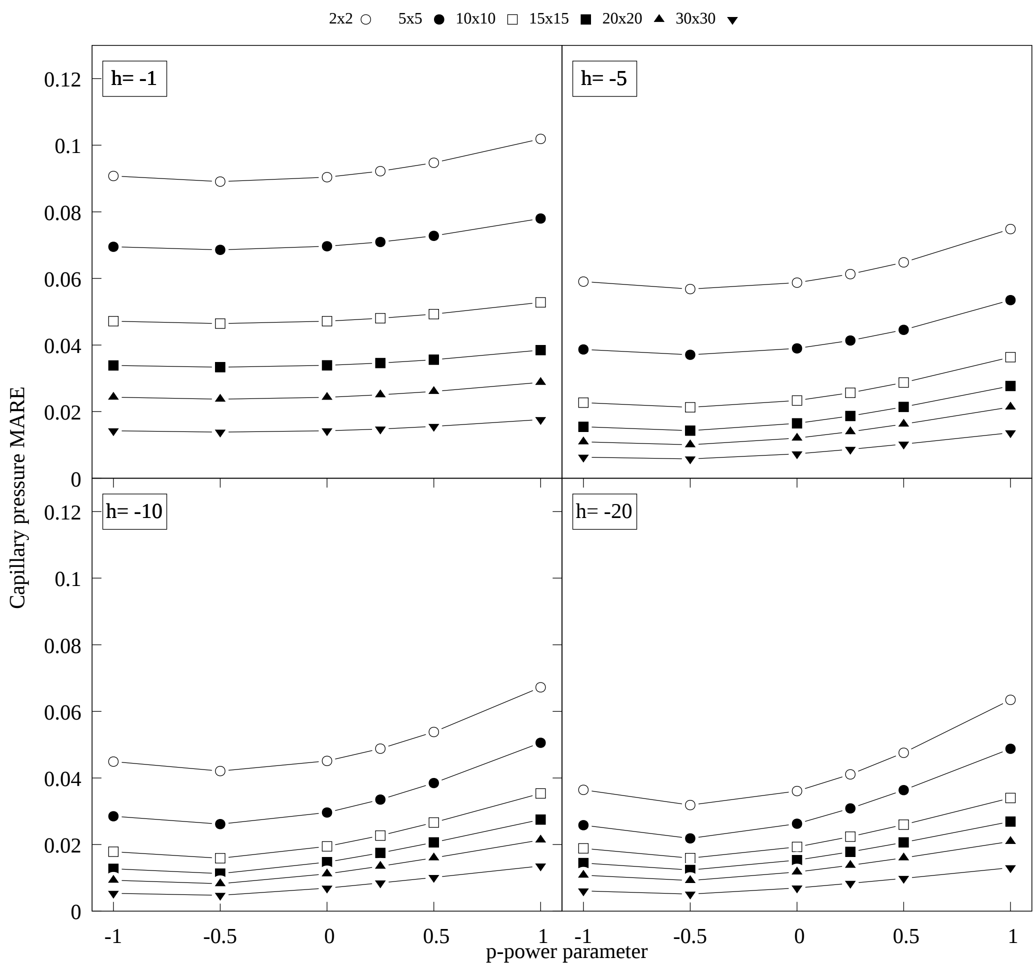

Figure B-1.: Capillary pressure MARE for non-Gaussian fields α=1.9

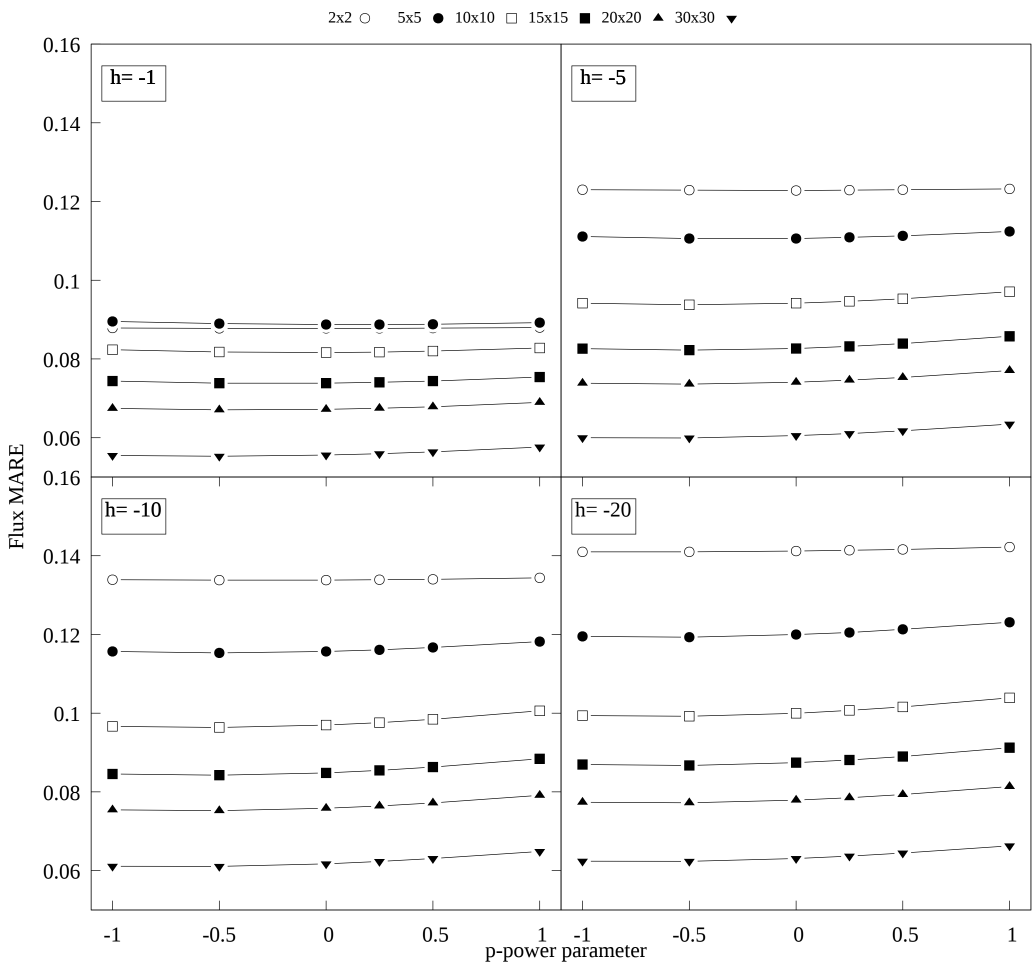

Figure B-2.: flux MARE for non-Gaussian fields α=1.9

B.2. Non-Gaussian fields α=1.7

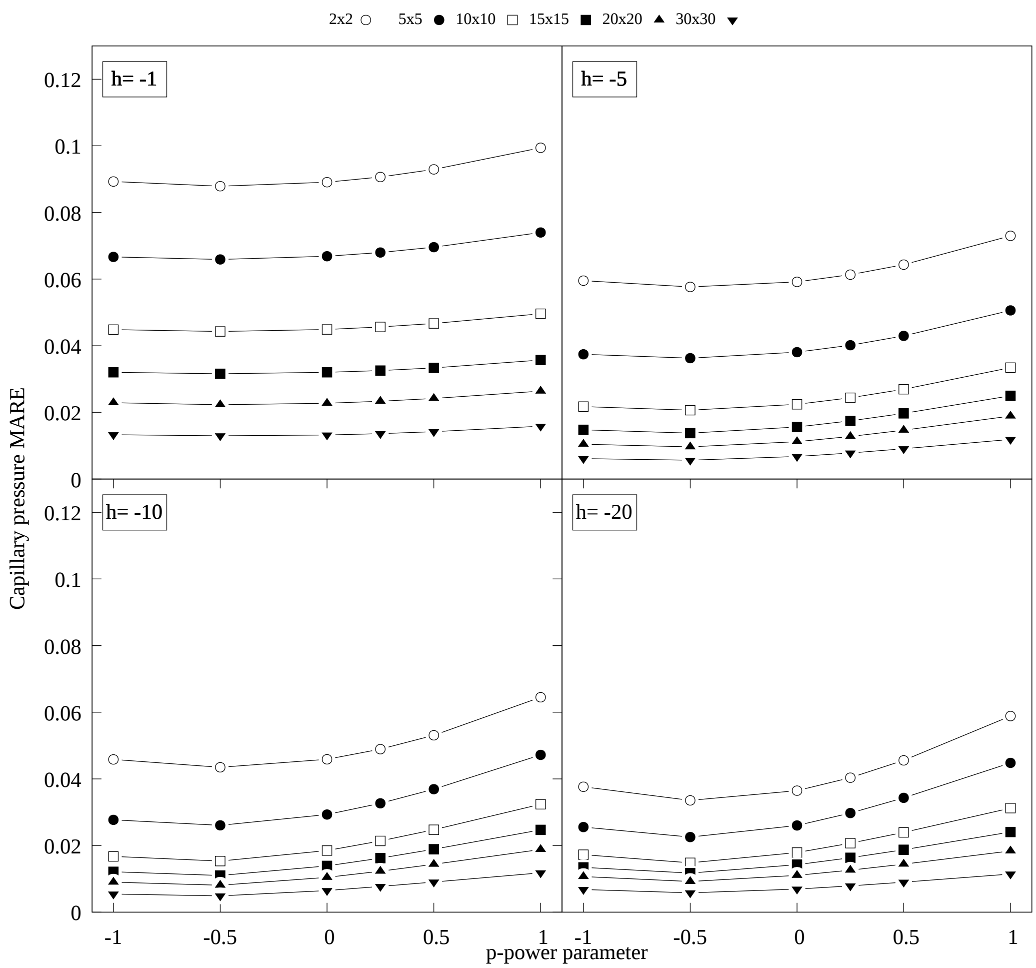

Figure B-3.: Capillary pressure MARE for non-Gaussian fields α=1.7

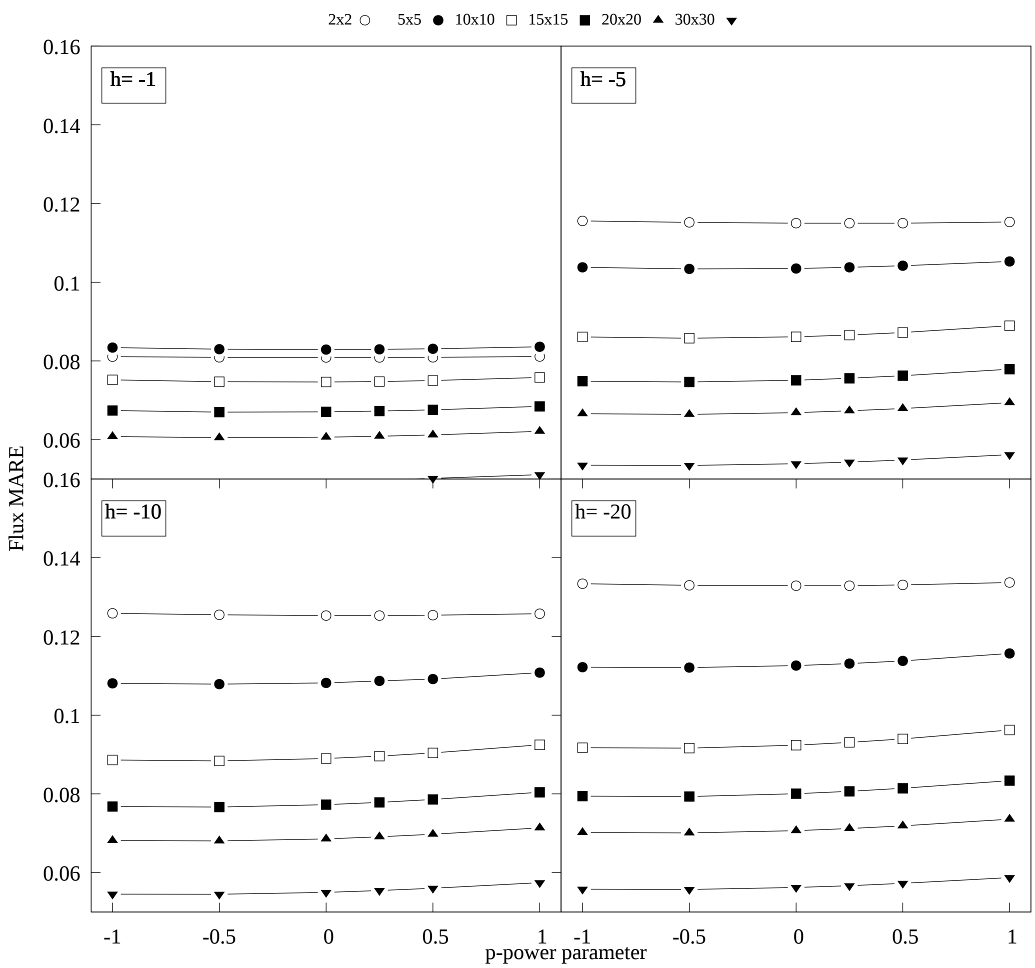

Figure B-4.: flux MARE for non-Gaussian fields α=1.7

B.3. Non-Gaussian fields α=1.5

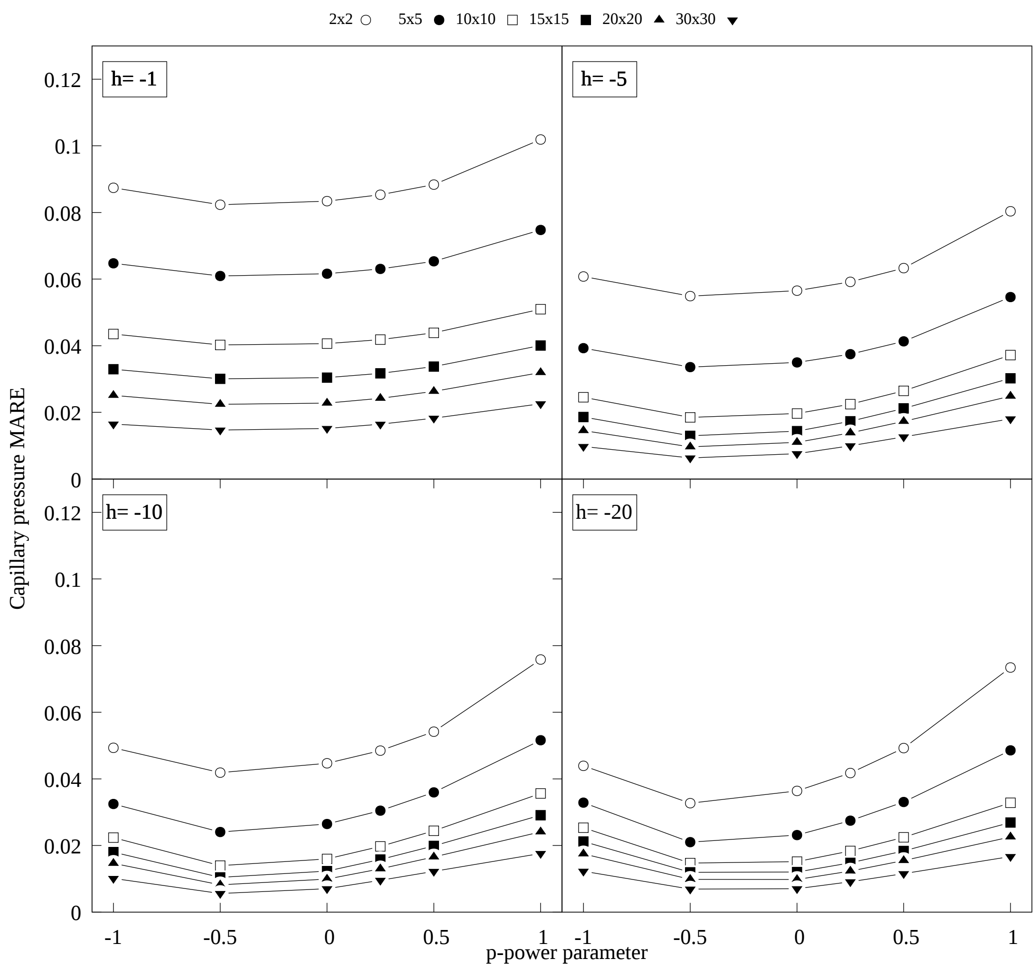

Figure B-5.: Capillary pressure MARE for non-Gaussian fields α=1.5

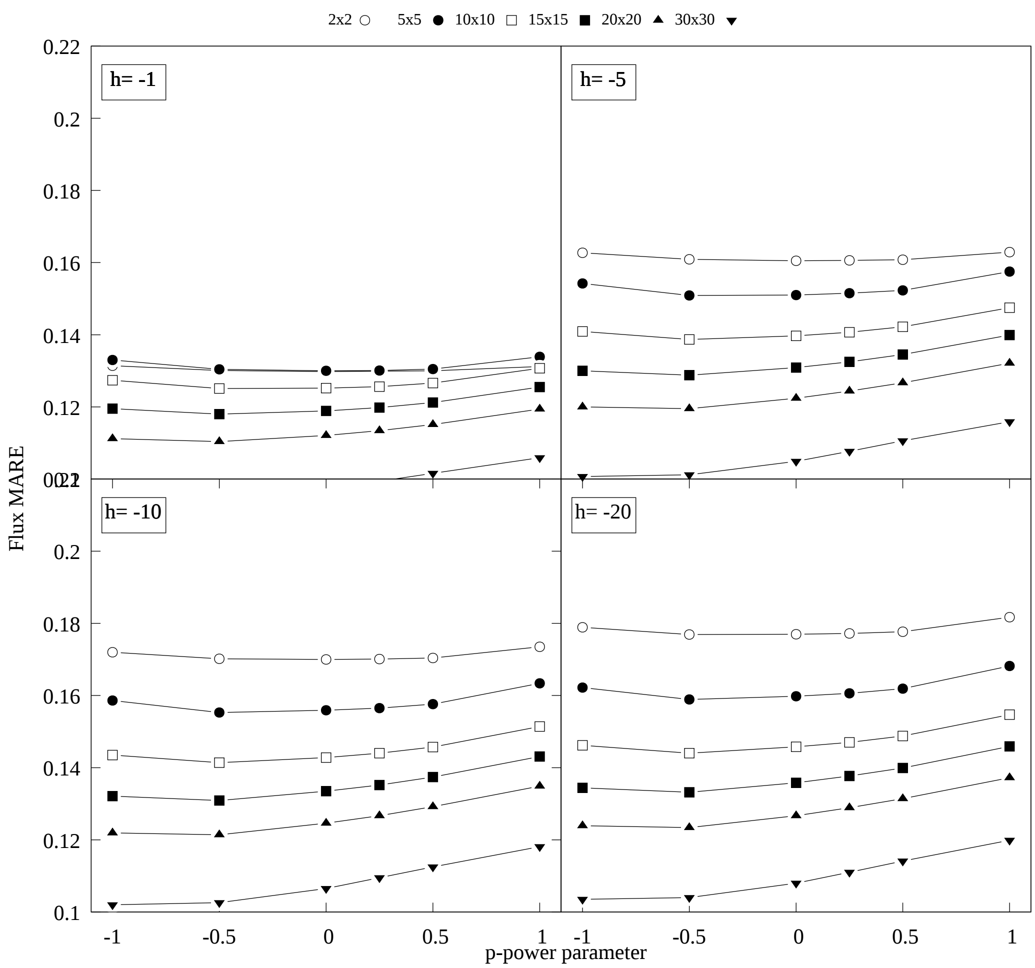

Figure B-6.: flux MARE for non-Gaussian fields α=1.5

B.4. Non-Gaussian fields α=1.3

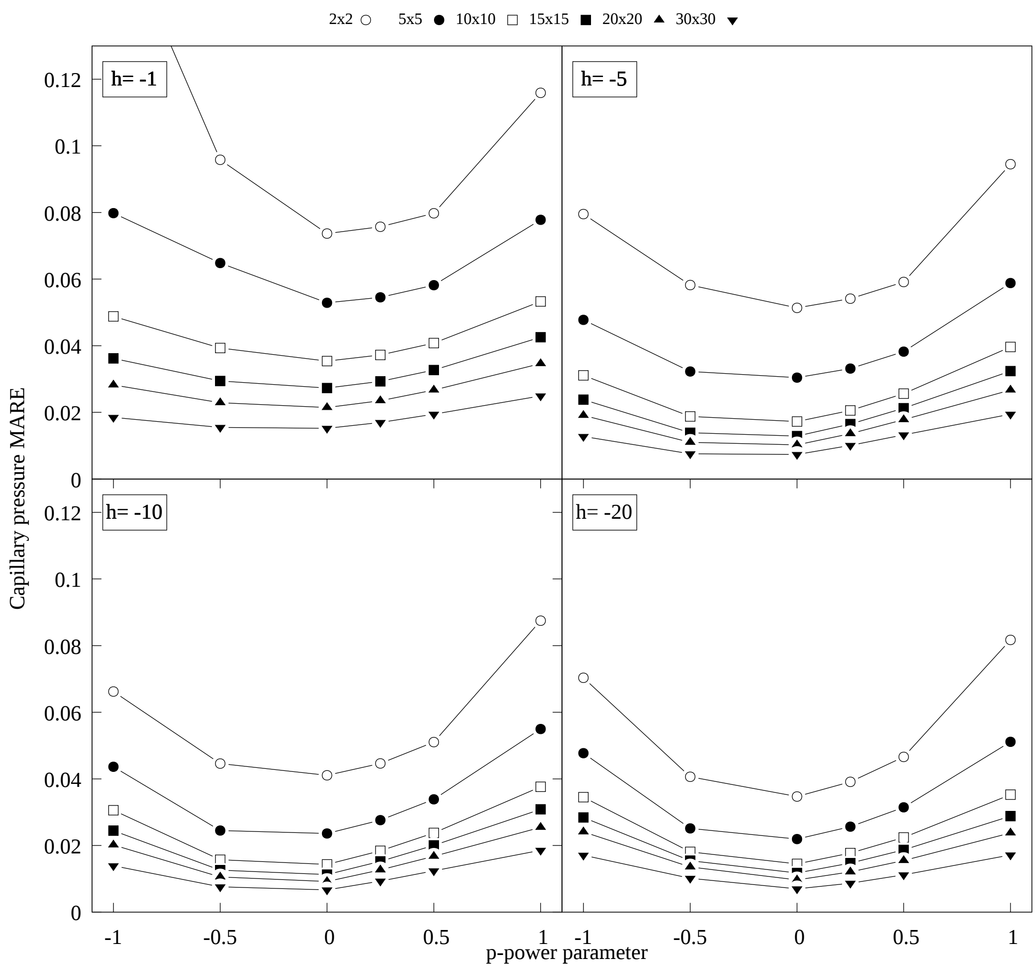

Figure B-7.: Capillary pressure MARE for non-Gaussian fields α=1.3

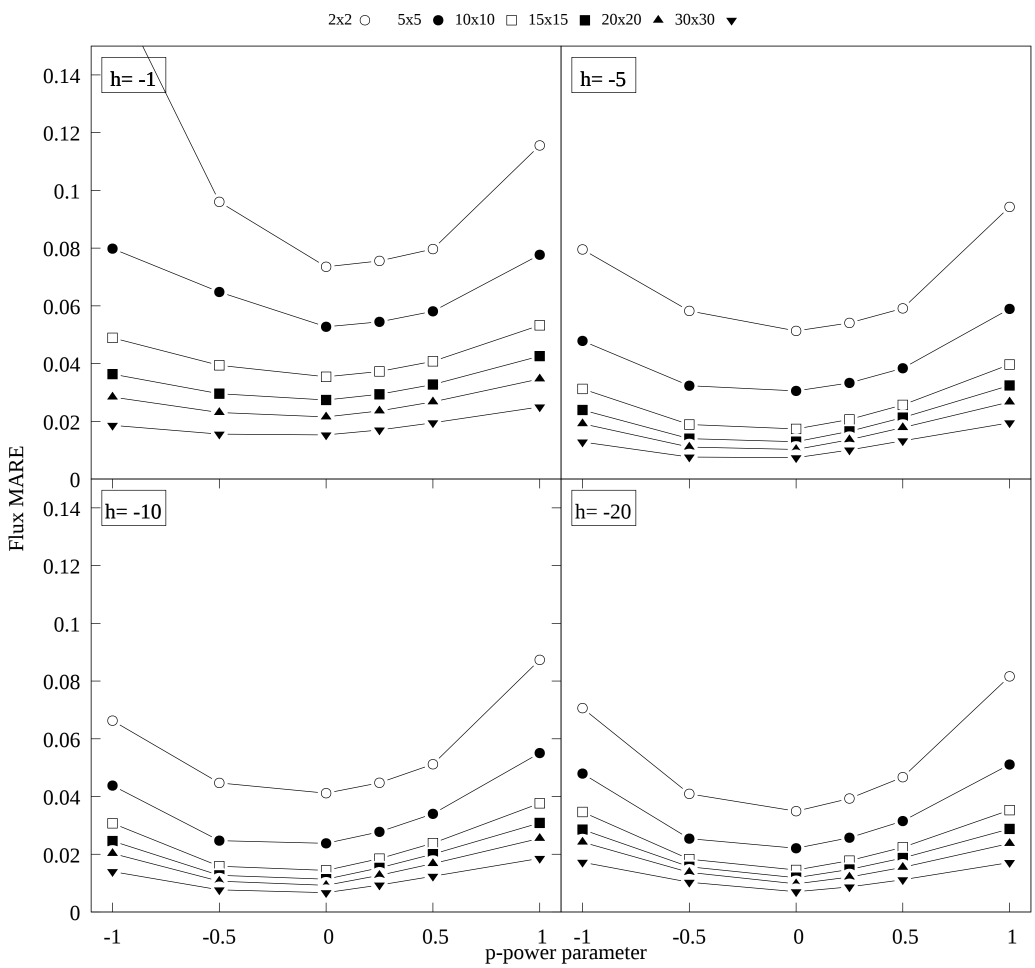

Figure B-8.: flux MARE for non-Gaussian fields α=1.3

References

Bear, J. (2012). *Hydraulics of groundwater.* Dover Publications.

Brooks, R. H., & Corey, A. T. (1964). *Hydraulic properties of porous media.* Colorado state university.

Celia, M. A., Bouloutas, E. T., & Zarba, R. L. (1990). A general mass-conservative numerical solution for the unsaturated flow equation. *Water Resources Research*, *26*(7), 1483-1496.

Darcy, H. (1856). *Les fontaines publiques de la ville de dijon: Exposition et application des principes a suivre et des formules a employer dans les questions de distribution d'eau; ouvrage terminé par un appendice relatif aux fournitures d'eau de plusieurs villes au filtrage des eaux et a la fabrication des tuyaux de fonte, de plomb, de tole et de bitume.* Victor Dalmont, Libraire des Corps imperiaux des ponts et chaussées et des mines.

Deutsch, C., & Journel, A. (1998). *Gslib geostatistical software library and user's guide.* Oxford University Press.

Domenico, P., & Schwartz, F. (1997). *Physical and chemical hydrogeology.* John Wiley & Sons, Inc.

Ferziger, J., & Peric, M. (2002). *Computational methods for fluid dynamics.* Springer.

Fetter, C. W. (1994). *Applied hydrogeology.* Prentice Hall.

Godoy, V. A., Zuquette, L. V., & Gómez-Hernandez, J. J. (2018). Stochastic analysis of three-dimensional hydraulic conductivity upscaling in a heterogeneous tropical soil. *Computers and Geotechnics*, *100*, 174-187.

Guadagnini, A., Riva, M., & Neuman, S. P. (2018). Recent advances in scalable non-gaussian geostatistics: The generalized sub-gaussian model. *Journal of Hydrology*, *562*, 685-691. doi: https://doi.org/10.1016/j.jhydrol.2018.05.001

Khaleel, R. (1999). *Far field hydrology data package for immobilized low acquitivity tank waste performance assessment, hnf4769* (Tech. Rep.). Pacific Northwest National Laboratory.

Khaleel, R., Yeh, T., & Lu, Z. (2002). Upscaled flow and transport properties for heterogeneous unsaturated media. *Water Resources Research*, *38*(5), 11 1 11 12.

Lichtner, P. C., Hammond, G. E., Lu, C., Karra, S., Bisht, G., Andre, B., ... Frederick, J. M. (2017a). *PFLOTRAN user manual* (Tech. Rep.). (http://www.documentation.pflotran.org)

Lichtner, P. C., Hammond, G. E., Lu, C., Karra, S., Bisht, G., Andre, B., ... Frederick, J. M. (2017b). *PFLOTRAN Web page.* (http://www.pflotran.org)

Liu, H. H., & Molz, F. J. (1997). Comment on evidence for non-gaussian scaling behavior in heterogeneous sedimentary formations by scott painter. *Water Resources Research*, *33*(4), 907-908. doi: 10.1029/96WR03788

Mualem, Y. (1976). A new model for predicting the hydraulic conductivity of unsaturated porous media. *Water Resources Research*, *12*(3), 513-522.

Painter, S. (1986). Evidence for non-gaussian scaling behavior in heterogeneous sedimentary formations. *Water Resources Research*, *32*(5), 1183-1195. doi: 10.1029/96WR00286

Richards, L. (1931). Capillary conduction of liquids through porous mediums. *Journal of Applied Physics*, *1*(5), 318-333.

Riva, M., Guadagnini, A., & Neuman, S. (2017). Theoretical analysis of non-gaussian heterogeneity effects on subsurface flow and transport. *Water Resources Research*, *53*, 2998-3012.

Riva, M., Neuman, S., & Guadagnini, A. (2015). New scaling model for variables and increments with heavy-tailed distributions. *Water Resources Research*, *51*, 4623-4634.

Riva, M., Neuman, S. P., Guadagnini, A., & Siena, M. (2013). Anisotropic scaling of berea sandstone log air permeability statistics. *Vadose Zone Journal*, *12*(3), vzj2012.0153. doi: 10.2136/vzj2012.0153

Rubin, Y. (2003). *Applied stochastic hydrogeology.* Oxford University Press.

Samper, F. J., & Carrera, J. (1990). Geoestadística: aplicaciones a la hidrología subterránea.

Tindall, J., & Kunkel, J. (1999). *Unsaturated zone hydrology for scientists and engineers.* Prentice Hall.

Van Genuchten, M. (1980, 09). A closed-form equation for predicting the hydraulic conductivity of unsaturated soils1. , *44*.

Wen, X.-H., & Gomez-Hernandez, J. J. (1996). Upscaling hydraulic conductivities in heterogeneous media: An overview. *Journal of Hydrology*, *183*(1), ix - xxxii. doi: https://doi.org/10.1016/S0022-1694(96)80030-8